scientific reports

Check for updates

OPEN

Optimizing agricultural biomass selection for biochar production using multicriteria decision-making

Ayodeji Raphael Ige[1]✉, Grażyna Łaska[1], Grzegorz Świderski[1] & Grzegorz Zając[2]

This study presents a multicriteria decision-making approach using the AHP-TOPSIS method to evaluate agricultural biomass for sustainable biochar production. Given the increasing demand for eco-friendly soil amendments, water treatment efficiency and renewable energy sources, identifying optimal agricultural biomass feedstocks is crucial. Key factors influencing biochar quality, including lignin content, carbon content, and nitrogen content, were prioritized during the selection process. A comprehensive evaluation was conducted, incorporating proximate analyses, Fourier Transform Infrared Spectroscopy (FTIR), and heating value assessments to verify the beneficial properties of various agricultural biomass types. After selecting the most suitable biomass of each kind, Thermogravimetric Analysis was employed to explore the thermal behaviour and biochar production potential of the selected materials. The results revealed that *Fraxinus excelsior* stood out with 18.16% lignin, 46.77% carbon, 0.52% nitrogen, 1.35% moisture content, and a calorific value of 20.24 MJ/kg, surpassing other samples. FTIR analysis confirmed the presence of functional groups in Fraxinus excelsior that enhances biochar stability. Furthermore, a combination of *Fraxinus excelsior* and Triticale demonstrated excellent thermal behaviour in Thermogravimetric Analysis, showing the highest residual mass at 760.5 °C (29.26%). These findings highlight that agricultural biomass not only offers favourable chemical and thermal properties but also contributes to sustainability by utilizing agricultural waste.

Keywords Biomass, Proximate, Lignin, Carbon, Multi-Criteria Decision-Making, Biochar

Addressing global warming requires the implementation of proactive climate and energy policies. Significant efforts must be made to curb greenhouse gas emissions and prevent further temperature increases. The European Union's climate strategy targets a 20% reduction in emissions compared to 1990 levels[1]. Achieving this goal necessitates a greater reliance on renewable energy sources[2]. The EU has sufficient biomass potential to expand its use in heating, district heating, and combined heat and power (CHP) industries, increasing from 5.2 to 67.3 million tons[3]. The industrial and energy sectors are the primary contributors to CO_2 emissions. Mandova et al.[4] suggest that EU iron and steel facilities could reduce emissions by 42% through biomass utilization, though this estimate may be optimistic. Their study highlights the potential of biomass, including waste-derived feedstock, while acknowledging technical constraints. Similarly, Giuntoli et al.[5] propose that incorporating cereal straw and cattle slurry in EU power generation could help mitigate global warming.

Agricultural biomass, derived directly from farming activities, includes cereal grains, sugar crops, oilseeds, field crops, and residues such as straw, grasses, and cultivated trees like willow and poplar. It also encompasses livestock byproducts, including manure and animal fats. Globally, wood and food waste are the most common forms of agricultural biomass[6]. Due to its varied physicochemical properties, agricultural biomass supports a broad range of applications[7]. Approximately 75% of agricultural biomass and residues of 384 Mt/and 323 Mt/a, respectively, originate from seven EU Member States: France, Germany, Poland, Italy, Spain, the UK, and Romania, with Poland primarily producing cereals and fodder crops[8].

Biochar, a carbon-rich, highly porous material resistant to decomposition, is produced through the thermal breakdown of plant or animal biomass in a low-oxygen environment[9]. It has garnered increasing attention for its agricultural and industrial applications. The physicochemical properties of biochar vary significantly, affecting its suitability for different uses[10]. Recent studies indicate that both its composition and production method influence key characteristics such as elemental composition, density, porosity, and pH are factors that determine

[1]Faculty of Civil Engineering and Environmental Sciences, Białystok University of Technology, Wiejska 45E, Białystok 15-351, Poland. [2]Faculty of Production Engineering, University of Life Sciences in Lublin, Gleboka 28, Lublin 20- 612, Poland. ✉email: ayodeji.ige@sd.pb.edu.pl

its effectiveness in various fields. Pyrolysis, a thermochemical process that decomposes organic feedstock under low or oxygen-free conditions, remains the predominant method for biochar production[11].

Multi-Criteria Decision-Making (MCDM) techniques provide a flexible framework for evaluating multiple variables using diverse methods, aiding decision-makers in analyzing complex issues[12]. Selecting suitable agricultural biomass for biochar production involves several critical factors, including resource availability, environmental impact, and production efficiency. As a result, this selection process is classified as a multi-criteria decision-making challenge that requires the consideration of multiple criteria and sub-criteria[13]. Among MCDM methodologies, the Analytical Hierarchy Process (AHP) is one of the most widely used tools[14]. A key advantage of AHP is its pairwise comparison approach, which enhances decision-making. However, traditional AHP does not fully capture human cognitive processes, presenting a notable limitation[15]. To address the inherent uncertainty in human judgment, Zadeh[16] introduced fuzzy set theory, enabling the use of linguistic expressions for more accurate subjective evaluations. The integration of fuzzy logic with AHP, known as the Fuzzy Analytical Hierarchy Process (FAHP), has gained widespread adoption across various engineering disciplines[13]. Numerous studies have applied the Technique for Order of Preference by Similarity to Ideal Solution (TOPSIS) or the AHP-TOPSIS methods to address selection challenges across different fields. Hanine et al.[17] implemented an integrated AHP-TOPSIS approach for ETL software selection, while Sivalingam and Subramaniam[18] employed a hybrid AHP-TOPSIS method for selecting cobots in the fuel filter assembly. Amiri et al.[19] developed a strategic MCDM framework for selecting renewable energy sources in Saudi Arabia using AHP-TOPSIS. Additionally, Zoma and Sawadogo[20] utilized a hybrid AHP-TOPSIS model to assess and select biomass availability for energy production in Burkina Faso.

The FAHP-TOPSIS approach has been widely applied in various fields but has yet to be used in biomass selection for biochar production. This study presents a combined FAHP-TOPSIS multicriteria decision-making approach to evaluate and prioritize agricultural biomass feedstocks for sustainable biochar production. Unlike previous studies, which largely focused on either chemical or thermal evaluations, this work distinctively merges detailed proximate and ultimate analyses, FTIR spectroscopy, and thermogravimetric validation within a robust decision-making framework. Its originality lies in the integration of comprehensive material characterization with an optimized decision model, effectively addressing the critical gap between biomass resource availability and the sustainable deployment of biochar.

The importance of this research is demonstrated by its direct support for eco-friendly waste valorization strategies, offering valuable insights into improving soil quality, enhancing carbon sequestration, and advancing circular agricultural practices. Moreover, the adaptability of the proposed methodology enables its application to broader areas, such as biomass selection for renewable energy, sustainable material innovations, and climate-resilient agricultural initiatives. Given the widespread availability of agricultural residues globally, the approach outlined in this study shows significant promise for adoption across diverse regions and socio-economic environments, contributing meaningfully to wider environmental management and sustainability goals.

Results

Ranking of agricultural biomass material by FAHP-TOPSIS

This stage aims to establish key evaluation criteria based on the properties of the selected biomass. For this study, the criteria include lignin, cellulose, hemicellulose, and the contents of carbon, hydrogen, nitrogen, sulfur, and oxygen. High levels of lignin, carbon, and nitrogen are considered beneficial, indicating favourable conditions for optimal performance. Xu et al.[21] found that increased nitrogen content in biomass leads to higher nitrogen levels in biochar, which is advantageous for applications like pollutant adsorption, catalysis, and energy storage[22]. Additionally, greater carbon content improves biochar production, enhancing its energy density, durability, and potential as a carbon-rich soil amendment or adsorbent[23]. Lignin is the primary precursor for biochar, significantly contributing to biochar yield[24].

In contrast, low levels of cellulose, hemicellulose, hydrogen, sulphur, and oxygen are considered unfavourable, with reduced values being preferable. According to Villa-Boas et al.[25] biomass with higher cellulose and hemicellulose content generally produces greater bio-oil yields, whereas biomass rich in lignin is suitable for biochar production due to the non-beneficial nature of cellulose and hemicellulose in this process. The presence of oxygen during pyrolysis negatively affects biochar yield and properties[26]. Elemental sulphur lowers biochar pH, making it a suitable amendment for arid lands by increasing soluble cations and reducing biochar's basicity and buffering capacity[27]. Sulphur-functional groups can be introduced through biomass selection, but the naturally low sulphur content in samples necessitates S-doping or post-treatment, which poses engineering challenges, making sulphur content less beneficial. Increasing carbon content leads to a reduction in hydrogen and oxygen levels, and pyrolysis can elevate carbon content to approximately 90% while significantly reducing hydrogen and oxygen[28] rendering hydrogen non-beneficial.

The pairwise comparison matrix is shown in Table 1, and the defuzzified crisp weights are provided in Table 2. A model for prioritization is created by assigning weights to different parameters and ranking them, enabling the identification and categorization of key factors while considering specific system outcomes. This performance model is developed using the AHP–TOPSIS method, which simplifies complex issues into an understandable format, resulting in a single performance score that reflects the prioritization of outcomes. As described earlier, the AHP method is used to determine the weights for various criteria that influence system performance. These weights are then incorporated into the TOPSIS framework to rank the individual parameters. This process ultimately produces performance scores for various agricultural biomasses, ranking them from most to least favourable. The consistency of the judgments was verified by calculating the Consistency Ratio (CR), which is the ratio of the Consistency Index (CI) to the appropriate value of the Random Consistency Index (RCI) as presented in Table 3. The CR is deemed acceptable since it does not exceed 0.10. The first step in this approach involves creating a normalized matrix by standardizing the properties of the biomass materials, as shown in

Samples (%)	Cellulose (%)	Hemicellulose (%)	Lignin (%)	Carbon (%)	Hydrogen (%)	Nitrogen (%)	Sulphur (%)	Oxygen (%)
Cellulose	1	2	0.5	0.2	2	0.5	5	4
Hemicellulose	0.2	1	0.11	0.11	1	0.3	2	1
Lignin	3	7	1	0.11	4	1	5	2
Carbon	5	7	4	1	7	7	9	7
Hydrogen	4	1	0.25	0.14	1	0.33	2	1
Nitrogen	2	3	1	0.14	3	1	2	2
Sulphur	0.2	0.5	0.2	0.11	0.5	0.2	1	0.5
Oxygen	0.25	1	0.33	0.14	1	0.33	2	1

Table 1. Pairwise comparison and result of FAHP.

	Defuzzified crisp weights
C1	0.308429
C2	0.122237
C3	0.503741
C4	1.317665
C5	0.275083
C6	0.335123
C7	0.07522
C8	0.133068

Table 2. Defuzzified crisp weights.

λmax	CI	RCI	CR
8.67489	0.0964	1.41	0.068

Table 3. Consistency checking.

Material	Cellulose	Hemicellulose	Lignin	Carbon	Hydrogen	Nitrogen	Sulphur	Oxygen
Fraxinus excelsior	0.480244	0.234034	0.457712	0.349944	0.325342	0.101256	0.076632	0.325413
Acer platanoides	0.49945	0.220899	0.451915	0.343509	0.331607	0.095414	0.102176	0.330714
Tilia cordata	0.477061	0.225938	0.451915	0.343884	0.328474	0.068153	0.051088	0.331932
Spelt bran	0.045806	0.443449	0.165593	0.312757	0.35264	0.547172	0.536426	0.338237
Oat bran	0.038719	0.43808	0.118461	0.31605	0.364275	0.408919	0.536426	0.338953
Wheat bran	0.041287	0.452619	0.183488	0.310962	0.351745	0.551067	0.485338	0.34053
Potato peel	0.427146	0.060553	0.391425	0.352787	0.315049	0.397235	0.019158	0.322045
Rye straw	0.168229	0.339692	0.319592	0.314254	0.313259	0.128517	0.408706	0.350488
Triticale straw	0.276171	0.364557	0.227092	0.351665	0.313259	0.177198	0.051088	0.320541

Table 4. Normalized decision matrix for agricultural biomass material selection.

Table 4. The next step in the TOPSIS process is calculating the weighted normalized decision matrix using the FAHP criteria weights, as outlined in Table 5.

In the next phase, the sum of both positive and negative deviations from the average solution was calculated. To appropriately prioritize agricultural biomass products, the closeness coefficient values were used to derive the final assessment score for each agricultural biomass type. In the final step, the agricultural biomass materials were ranked based on their relative proximity. The ranking order is as follows: 7-8-9-3-4-1-2-6-5. *Fraxinus excelsior* was selected from wood residues, potato peels and wheat bran were chosen from food waste, and triticale straw was picked from crop residues, as shown in Table 6.

Proximate and calorific values

Table 7 presents the results of the proximate analysis and calorific values for various agricultural biomass samples. *Fraxinus excelsior* exhibited the lowest moisture content at 1.35%, which was lower than all other wood residue samples. Similarly, potato Peel had a moisture content of 3.78%, lower than other food waste

Material	Cellulose	Hemicellulose	Lignin	Carbon	Hydrogen	Nitrogen	Sulphur	Oxygen
Fraxinus excelsior	0.148121	0.028608	0.230568	0.461109	0.089496	0.033933	0.005764	0.043302
Acer platanoides	0.154045	0.027002	0.227648	0.45263	0.091219	0.031976	0.007686	0.044007
Tilia cordata	0.147139	0.027618	0.227648	0.453123	0.090358	0.02284	0.003843	0.04417
Spelt bran	0.014128	0.054206	0.083416	0.41211	0.097005	0.18337	0.04035	0.045009
Oat bran	0.011942	0.05355	0.059674	0.416448	0.100206	0.137038	0.04035	0.045104
Wheat bran	0.012734	0.055327	0.092431	0.409743	0.096759	0.184675	0.036507	0.045314
Potato peel	0.131744	0.007402	0.197177	0.464856	0.086665	0.133123	0.001441	0.042854
Rye straw	0.051887	0.041523	0.160992	0.414081	0.086172	0.043069	0.030743	0.046639
Triticale straw	0.085179	0.044562	0.114395	0.463377	0.086172	0.059383	0.003843	0.042654

Table 5. Weighted normalized decision matrix for agricultural biomass material selection.

Types of material	Material	Si+	Si-	CI	Ranking	Selection
Wood residue	*Fraxinus excelsior*	0.214758	0.434211	0.669078	7	Selected
	Acer platanoides	0.220942	0.429582	0.660363	8	
	Tilia cordata	0.22344	0.43286	0.659546	9	
Food waste	Spelt bran	0.127011	0.418509	0.767175	3	
	Oat bran	0.1507	0.403178	0.727918	4	
	Wheat bran	0.122694	0.422916	0.775125	1	Selected
	Potato peel	0.13403	0.443566	0.767952	2	Selected
Crop residue	Rye straw	0.173612	0.39434	0.694319	6	
	Triticale straw	0.159648	0.413402	0.721407	5	Selected

Table 6. Appraisal score and corresponding rank.

Sample	Moisture content (%)	Volatile matter (%)	Ash content (%)	Fixed carbon (%)	HHV (MJ/kg)	LHV (MJ/kg)
Fraxinus excelsior	1.35	76.87	5.41	16.37	20.24	18.61
Acer platanoides	1.38	79.96	5.00	13.66	19.50	17.87
Tilia cordata	1.55	78.98	3.95	15.52	20.01	18.38
Spelt bran	4.22	70.18	9.67	15.93	17.18	15.64
Oat bran	4.13	73.57	5.89	16.41	19.44	17.84
Wheat bran	4.88	69.66	7.6	17.86	19.11	17.58
Potato peel	3.78	69.69	8.85	17.68	17.39	15.84
Rye straw	1.56	74.69	9.20	14.55	18.37	16.77
Triticale straw	1.49	73.06	9.95	15.5	19.16	17.55

Table 7. Proximate analysis and calorific values of the agricultural biomass of dry basis.

samples, while triticale straw, at 1.49%, had a moisture level lower than that of Rye straw, as shown in Table 7. With the moisture content of these agricultural biomasses falling below the acceptable threshold of 10%, they are considered suitable for thermal utilization, making them promising feedstock for energy generation[29]. The moisture content of biomass plays a crucial role in pyrolysis efficiency and product yield. High moisture levels reduce the thermal energy available for pyrolysis, resulting in lower Biochar yields and higher energy consumption for drying. Additionally, excessive moisture requires more drying units, increasing energy costs and overall process expenses[23]. *Fraxinus excelsior* also observed the lowest volatile matter (VM) content among wood residue biomass (76.87%), while wheat Bran exhibited the lowest VM content in food waste biomass (69.66%), and triticale straw had the lowest VM in crop residue biomass (73.06%), as indicated in Table 7. Furthermore, *Tilia cordata* displayed the lowest Ash content across all biomass samples. A higher volatile matter content in biomass generally indicates a higher potential for fuel ignition, which enhances bio-oil production, while a higher Ash content is undesirable due to its negative effects on combustion and gasification processes, hindering energy production. Factors such as soil type and irrigation water can also impact Ash content[30]. The fixed carbon content in biomass is another crucial factor in pyrolysis, as it directly affects Biochar yield and quality. Typically, a high fixed carbon content leads to greater Biochar production, which is valued for its energy density, stability, and potential as a carbon-rich soil amendment or adsorbent[29]. Calorific value is a key thermo-physical property that reflects the energy potential of materials and serves as an important indicator of their fuel quality. Among all agricultural biomass samples, spelt Bran exhibited the lowest high heating value (HHV) at

17.18 mj/kg and lower heating value (LHV) at 15.64 mj/kg, consistent with the findings for spelt chaff (18.68 and 16.78 MJ/kg) reported by Wiwart et al.[31]. The net calorific value is closely associated with moisture content and is significantly influenced by the chemical composition of the fuel[32].

FT-IR analysis

The FTIR ATR spectra for the *Fraxinus excelsior*, *Acer platanoides* and *Tilia cordata* samples are shown in Fig. 1. The wavenumbers of the characteristic bands present in the spectra and the band assignments are listed in Table 8. The bands present in the spectra were assigned based on literature data[33–36]. The recorded spectra of wood samples show many characteristic bands associated with the vibrations of fragments of lignin, cellulose and hemicellulose molecules[34,35]. The band originating from the stretching vibrations of the νC = O carbonyl group located at wavenumbers 1737 cm^{-1} (*Fraxinus excelsior*), 1739 cm^{-1} (*Acer paltanoides*) and 1739 (*Tilia cordata*) are characteristic of lignins occurring in wood[36,37]. The presence of this band may also be related to the content of carboxylic acids. Another band indicating a high content of lignin in the samples is the $\nu C = C_{ar}$ stretching band located at wavenumbers 1505–1507 cm^{-1} in the tested wood samples as presented in Table 11. The bands located at wavenumbers 1459–1457 cm^{-1} are bands associated with deformation/bending vibrations of CH_2, CH_3 bonds occurring in lignins and celluloses. In the range of 1239–1086 cm^{-1}, the recorded spectra contain bands associated with stretching vibrations of νC-O, νCOH, νC-O-C.

These are vibrations associated with the presence of celluloses, hemicelluloses and lignins in the tested samples. The deformation bands δCOH, δCCH, δOCH, present in the spectral range of 844–753 cm^{-1} originate from vibrations associated with the presence of polysaccharides in wood (mainly celluloses). The spectrum also contains bands of out-of-plane bending vibrations γCC_{ring}, γCH_{ring}, and deformation vibrations of the aromatic ring. The region of these bands is 666–657 cm^{-1}. The presence of aromatic ring vibrations is related to the presence of lignin and the possible content of other aromatic compounds in the samples.

In *Fraxinus excelsior*, the FTIR spectrum is consistent with its carbon content (46.77%) and hydrogen content (7.27%) as presented in Table 11, which reflect the structural organic components (lignin, hemicellulose, and cellulose). Additionally, the oxygen content (45.42%) agrees with the presence of C-O and C-O-C stretching vibrations, which are characteristic of cellulose and hemicellulose. The sulfur content (0.03%) is low, which is typical for these tree species and does not significantly interfere with the FTIR signals. For *Acer platanoides* (ACT), the FTIR spectra shows a reduced intensity for the hemicellulose-related peaks (such as C-H deformation and C-O stretching), corresponding to the lower hemicellulose content (26.74%). This reduction in hemicellulose aligns with the carbon content (45.91%) and hydrogen content (7.41%) of ACT, which also reflects its overall lower carbohydrate content. The strong C-O-C stretching band in the FTIR spectrum, reflecting the higher cellulose content (48.63%), corresponds with the observed higher carbon content in ACT. The oxygen content (46.16%) also supports the prevalence of cellulose and hemicellulose components, with oxygen being a critical element in these polysaccharides. Nitrogen content (0.49%) and sulfur content (0.04%) are low, consistent with the typical levels found in lignocellulosic materials and further corroborated by the FTIR spectra.

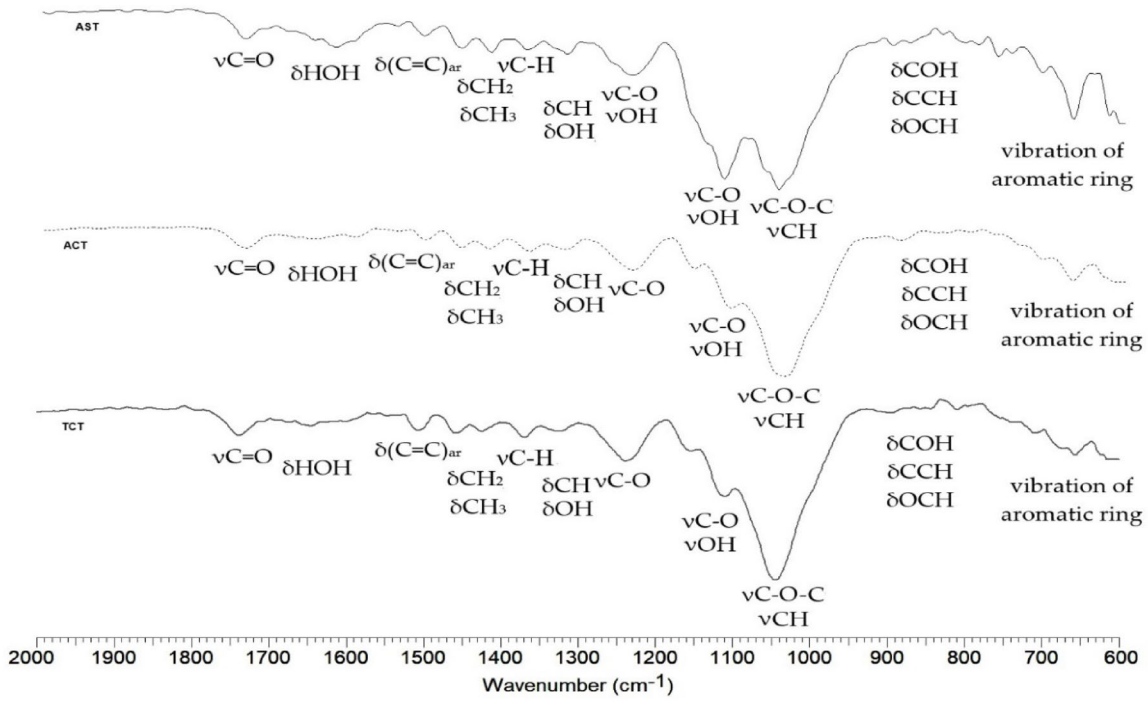

Fig. 1. FTIR ATR spectra of *Fraxinus excelsior* (AST), *Acer platanoides* (ACT) and *Tilia cordata* (TCT) recorded in the wavenumber range 2000 cm^{-1}–600 cm^{-1}.

Fraxinus excelsior	*Acer platanoides*	*Tilia cordata*	Type of vibration	Groups of chemical compounds
1737 m	1739 m	1739 m	νC = O	Carboxylic acid, lignin, hemicelulose
1620 m			δHOH	Cellulose
1505 m	1505 w	1507 w	$\delta C=C_{ar}$	Aromatic compound, lignin
1457 m	1459 w	1459 w	δCH_2, δCH_3	Cellulose, hemicellulose, lignin
1372 w	1371 w	1369 w	νC-H	Cellulose
1320 w	1324 w	1324 w	δCH, δOH	Cellulose, lignin
1236 m	1236 m	1239 m	νC-O, νC-C,	Carboxylic acid, cellulose, lignin
-	1157 m	1154 m	νC-O-C, δCH	Cellulose, hemicellulose, lignin
1119 vs.	1110 m	1110 m	νC-O, νOH	Cellulose, hemicellulose
1048 vs.	1041 vs.	1045 vs.	νC-O-C, νC-H	Cellulose, hemicellulose, lignin
899 w	891 w	898 w	δCH	Cellulose, hemicellulose
877 w			δCH	Aromatic compound, lignin
		858 w	δCH	Aromatic compound, lignin
835 w	844 w	844 w	δCOH, δCCH,	Polyssacharides/carbohydrates
789 w		796 w	δCOH, δCCH, δOCH	Polyssacharides/carbohydrates
666 s	667 m	673 w	γCC_{ring}, γCH_{ring}	Aromatic compound/lignin
639 m		657 m	γCC_{ring}, γCH_{ring}	Aromatic compound/lignin
620 m			def_{ring}	Aromatic compound/lignin

Table 8. Wavenumbers (cm^{-1}), intensities and assignments of bands occurring in the FTIR spectra of *Fraxinus excelsior*, *Acer planatoides* and *Tilia cordata*. Abbreviations: ν-streching, δ-deforming in plane, γ-deforming out of plane, def-deformation, ring- vibrations of atoms of an aromatic ring, intensities: vs-very strong, s-strong, m-medium, w-weak.

Tilia cordata (TCT), with a cellulose content of 46.45%, also shows prominent C-O-C stretching vibrations around 1154 cm^{-1} in the FTIR spectrum, confirming the high cellulose content. The elemental composition of TCT, with a carbon content of 45.96%, hydrogen content of 7.34%, and oxygen content of 46.33%, supports the FTIR findings. These components are characteristic of the lignocellulosic structure of TCT, with carbon and oxygen being integral to the cellulose and hemicellulose, and hydrogen being part of the polysaccharide structures. Nitrogen content (0.35%) and sulfur content (0.02%) in TCT are also low, which further corroborates the FTIR results, confirming the absence of significant non-organic compounds influencing the spectral peaks.

The FTIR ATR spectra for the spelt bran, oat bran, wheat bran and potato peel are shown in Fig. 2. The wavenumbers of the characteristic bands present in the spectra and the band assignments are listed in Table 9. The bands present in the spectra were assigned based on literature data[37–40]. Analysis of FTIR spectra of spelt bran, oat bran and wheat bran showed that these products contain compounds from the group of celluloses, lignin, hemicelluloses and polysaccharides. Moreover, characteristic amide bands are present in the tested samples, indicating the presence of proteins in the tested products. The amide band (I) associated with the stretching vibrations of the carbonyl group (νC = O) and the stretching vibrations of the νC-N group appear on the spectra at wave numbers 1740–1739 cm^{-1}. The amide band (II) associated with the stretching vibrations of the carbonyl group (aminoacids), the stretching vibrations of the νC-N bond and the stretching vibrations of the νC-H vibrations are present in the spectra in the wavenumber range from 1648 to 1645 cm^{-1}. The amide band (III) originates from the νC-N stretching vibrations and the NH bending vibrations is in the wavenumber range from 1243 to 1255 cm^{-1}. The amide bands (I-III) are also present in the potato peel spectrum, which indicates that this product also contains proteins. The intensity of the amide bands (I-III) in the potato peel spectrum is lower than the intensity of this band in the other samples, which indicates a lower protein content in this product. In the potato peel spectrum, the νC-O band was not observed at wavenumbers around 1700 cm^{-1}. This band is present on the spectra of the other three samples. It was also observed that the band originating from the νC-O-C stretching vibrations present in the bran spectra (located at wavenumber − 1151 cm^{-1}), has a high intensity, while in the potato peel spectrum the intensity of this band is lower. This may indicate a lower content of cellulose and hemicelluloses in the potato sample. The carbon content (47.15%) and hydrogen content (7.04%) are in good agreement with the FTIR peaks and makes it to have higher carbon content and lower oxygen content compared to other samples in the category of food waste as presented in Table 11, while the low sulfur content (0.0775%) further supports the reliability of the FTIR results as sulfur does not interfere with the spectra.

Figure 3 shows the FTIR spectra of Rye straw and Triticale straw. The wavenumbers of the bands present in the recorded spectra and their assignment are presented in Table 10. The bands present in the spectra were assigned based on literature data[41–43]. On the spectra of Rye straw and Triticale straw samples, a band was observed located at wave numbers of 1737 cm^{-1} and 1733 cm^{-1}, respectively. These bands correspond to the vibrations of carbonyl groups occurring in lignins, celluloses and hemicelluloses[42,43]. Cellulose can absorb water, as evidenced by the presence of a band originating from bending vibrations of δHOH at wave numbers of 1647 cm^{-1} and 1648 cm^{-1} in the recorded spectra[42]. Straw samples of the examined cereals are a rich source

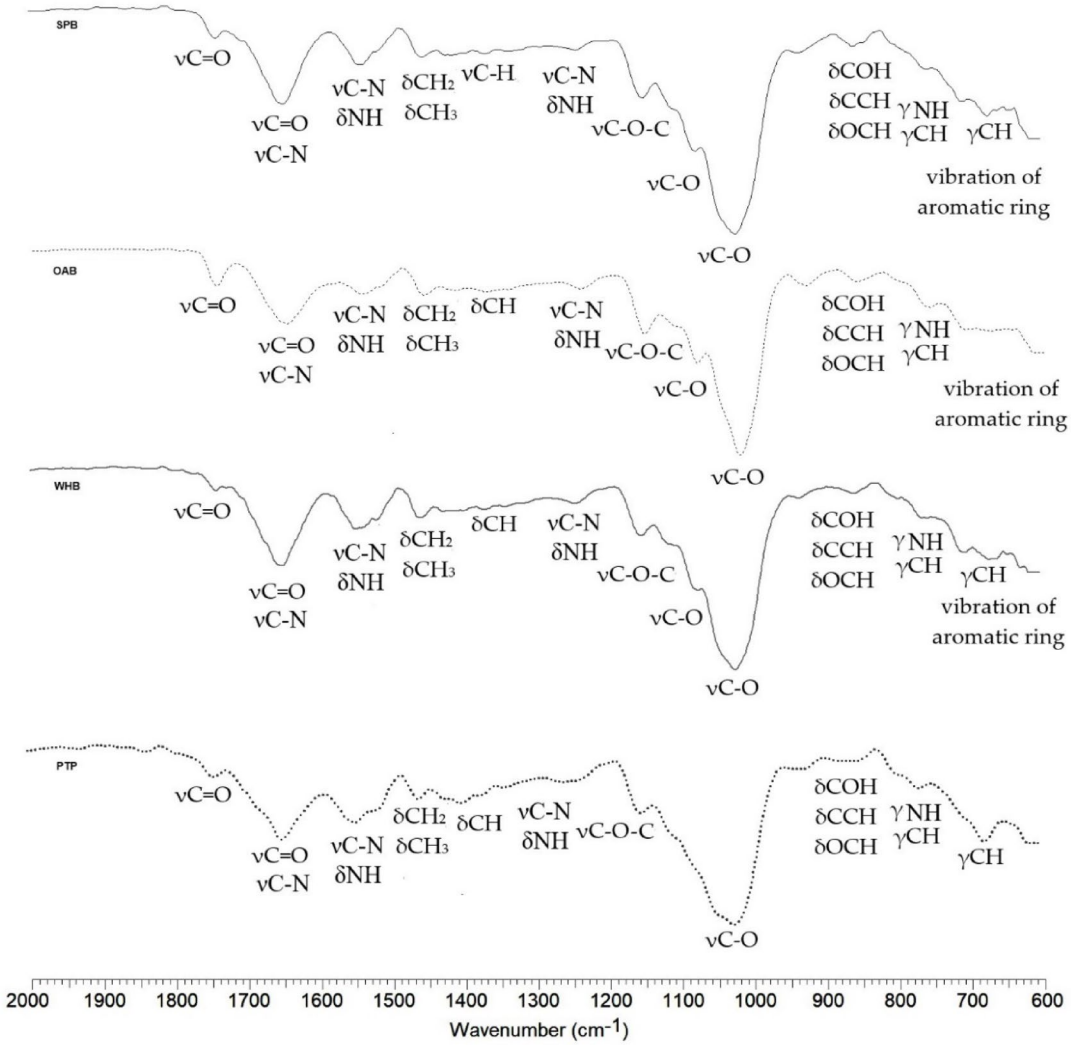

Fig. 2. FTIR ATR spectra of spelt bran (SPB), oat bran (OAB), wheat bran (WHB) and potato peel (PTP) recorded in the wavenumber range 2000 cm^{-1}–600 cm^{-1}.

of lignins, cellulose and hemicelluloses, which is confirmed by FTIR spectroscopic analysis while the carbon, hydrogen, and oxygen elements are reflected in these peaks.

Another band appearing in the spectra characteristic for cellulose and lignin is the band associated with the bending vibrations of the -COH, OH groups and the deformation vibrations of the aromatic ring (lignin). This band is located at wave numbers 1426 cm^{-1} (Rye straw spectrum) and 1422 cm^{-1} (Triticale straw spectrum). In the range of wave numbers from 1369 cm^{-1} to 1243 cm^{-1}, bands associated with the stretching vibrations of νC-H, νC-O, νC-C and with the bending vibrations of δCOH, δOH were observed in the spectra. These bands are characteristic of the cellulose molecules present in the samples. In the range of wave numbers 899 cm^{-1} – 667 cm^{-1}, the bands of the deformation vibrations of the hydroxyl group δOH and the bands of the deformation vibrations of the C-H bonds are located. These are the bands characteristic of cellulose. The presence of lignins in the tested samples is confirmed by the occurrence of a many of bands in the recorded spectra. These include the stretching vibration bands νC-H, νC-O-C (1046 cm^{-1}), or the bending vibration bands δCH_2, δCH_3. These bands are characteristic of the lignins present in the samples, as well as celluloses and hemicelluloses[41–43]. The spectra of the Rye straw and Triticale straw samples are very similar to each other. The position of the bands in the spectra of both samples differ slightly. The straw of both cereals is characterized by a similar composition of biopolymer compounds.

Based on the analysis of FTIR ATR spectroscopic spectra recorded for wood and cereal straw samples, it can be stated that the tested products contain biopolymers from the group of celluloses, hemicelluloses and lignins and other polysaccharide compounds, as well as small amounts of aromatic compounds that cannot be identified on the recorded spectra. Bran and potato peel samples also contain compounds from the group of lignins, celluloses and hemicelluloses, and in addition, the presence of proteins was found in these samples. Characteristic amide bands are present in the spectra of these products, confirming the presence of proteins. Potato peels contain significantly less protein than bran. However, an increased content of carbohydrates can

Spelt bran	Oat bran	Wheat bran	Potato peel	Type of vibration	Groups of chemical compounds
1740 m	1743 m	1739 w	1739 m	νC = O	Carboxylic acid, lignin, hemicelulose
1647 s	1647 s	1648 s	1645 s	νC = O, νC-N, amide band I	Carboxylic acid/amino acid/proteins
1543 m	1545 m	1545 s	1543 s	δNH, νC-N, νC-H amide band II	Aminoacids/proteins
1456 m	1457 m	1457 m	1457 m	δCH_2, δCH_3	Cellulose, hemicellulose, lignin
1423 w	1415 w	1425 w	1417 w	δCOH, δOH, $\delta C = C_{ar}$	Cellulose, hemicellulose, lignin
	1369 w	1368 w	1372 w	νC-H	Cellulose, hemicellulose
1333 w	1341 w	1340 w	1338 w	δCH_2, δCH_3	Cellulose, hemicellulose, lignin
1241 m	1240 m	1243 m	1255 m	δNH, νC-N amide band III	Aminoacids/proteins
1151 s	1151 s	1151 s	1148 m	νC-O-C, δCH	Cellulose, hemicellulose, lignin
1078 m	1079 m	1072 m	-	νC-O	Hemicellulose, lignin
1022 vs.	1020 vs.	1021 vs.	1020 vs.	νC-O	Polysacharides
936 w	930 m	933 m	925 m	νC-O, νC-C	Polysacharides
860 m	858 m	858 m	851 w	δCOH, δCCH, δOCH	Polyssacharides/carbohydrates
756 w	756 w	756 w	765 m	γNH, γCH	Protein
708 w	709 w	705 m		γCC_{ring}, γCH_{ring}	Aromatic compound/lignin
673 m	671 w	670 m	674 w	γCC_{ring}, γCH_{ring}	Aromatic compound/lignin
602 w	602 w	602 w	602 w	def_{ring}	Aromatic compound

Table 9. Wavenumbers (cm^{-1}), intensities and assignments of bands occurring in the FTIR spectra of spelt Bran, oat Bran, wheat Bran and potato peel. Abbreviation: ν-streching, δ-deforming in plane, γ-deforming out of plane, def-deformation, ring- vibrations of atoms of an aromatic ring, intensities: vs-very strong, s-strong, m-medium, w-weak.

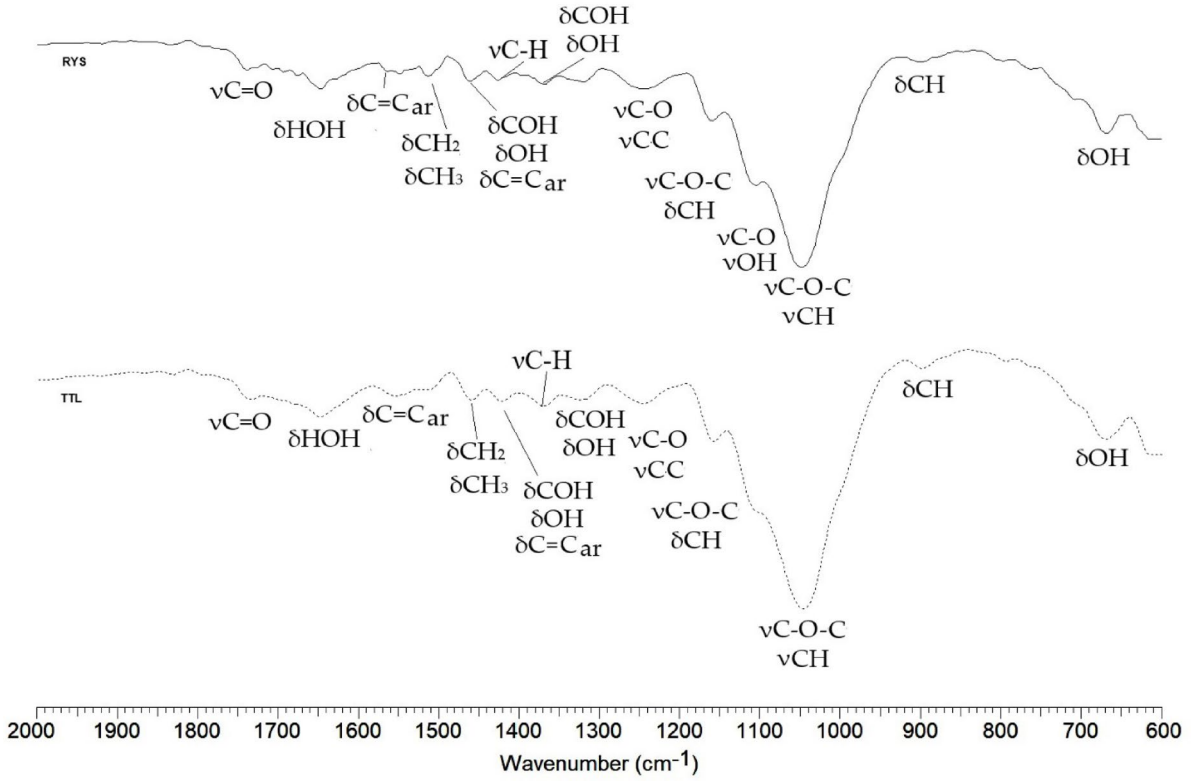

Fig. 3. FTIR ATR spectra of Rye straw (RYS), Triticale straw (TTL) recorded in the wavenumber range 2000 cm^{-1}–600 cm^{-1}.

Rye straw	Triticale straw	Type of vibration	Groups of chemical compounds
1737 m	1733 m	νC = O	Lignin, hemicellulose
1647 m	1648 m	δHOH	Cellulose
1548 w	1556 w	$\delta C = C_{ar}$	Aromatic compound, lignin
1460 m	1456 m	δCH_2, δCH_3	Cellulose, hemicellulose, lignin
1426 m	1422 m	δCOH, δOH, $\delta C = C_{ar}$	Cellulose, lignin
1368 m	1369 m	νC-H	Cellulose
1318 m	1323 m	δCOH, δOH,	Cellulose
1243 s	1246 s	νC-C, νC-O	Cellulose
1158 m	1158 m	νC-O-C, δCH	Cellulose, hemicellulose, lignin
1103 m	-	νC-O, νOH	Cellulose, hemicellulose
1046 vs.	1046 vs.	νC-H, νC-O-C	Lignin, cellulose, hemicellulose
899 m	898 m	δCH	Cellulose
854 w	-	δCH	Cellulose
667 m	670 w	δOH	Cellulose
602 w	602 w	γCC_{ring}, γCH_{ring}	Aromatic compound/lignin

Table 10. Wavenumbers (cm^{-1}), intensities and assignments of bands occurring in the FTIR spectra of Rye straw and Triticale straw. Abbreviations: ν-streching, δ-deforming in plane, γ-deforming out of plane, def-deformation, ring- vibrations of atoms of an aromatic ring, intensities: vs-very strong, s-strong, m-medium, w-weak.

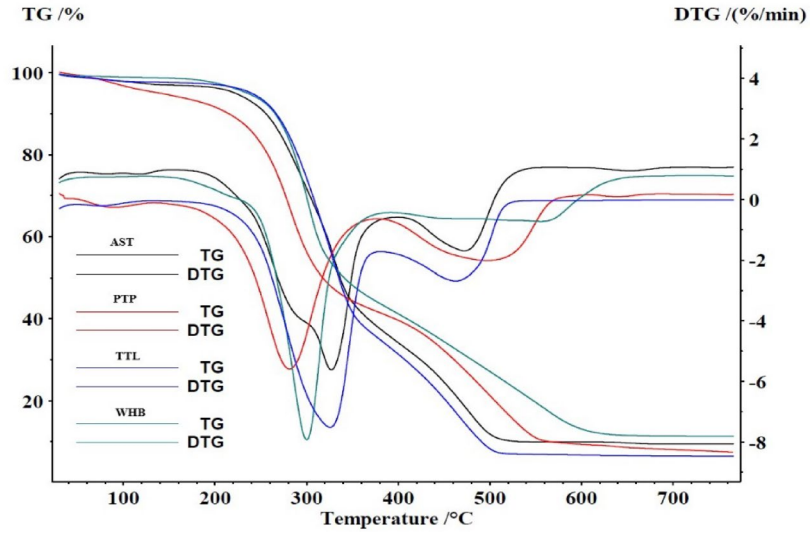

Fig. 4. TGA and DTG curve of AST, PTP, TTL and WHB.

be observed in the potato peel sample compared to the other samples. A precise analysis of the content of individual polymer compounds and their quantitative analysis is not possible using infrared spectroscopy. The tested samples may also contain several other organic and mineral compounds that were not observed due to the overlap of bands in the spectra.

Discussion

The results present thermogravimetry analysis of the selected agricultural biomass and blends in three steps: drying stage, devolatilization stage and char formation stage. Each stage presents the variation of moisture, volatile substances, and ash content in selected samples based on the specific ranking FAHP and TOPSIS processes (Table 6). Thermogravimetry analysis (TGA) and the derivative thermogravimetric (DTG) curves derived from the TGA curves for individual samples were: *Fraxinus excelsior* (AST) from wood residues, potato peels (PTP) and wheat bran (WHB) from food waste, and triticale straw from crop residues (TTL), and their different mixed described below (Figs. 4, 5, 6, 7, 8, 9 and 10).

Explanation of abbreviations for Fig. 6, 7, 8, 9, 10, 11 and 12, where:AST = *Fraxinus excelsior*; PTAS = Potato + *Fraxinus excelsior*; PTP = Potato peel; PTTL= Potato peel + Triticale; PTWH = Potato peel + Wheat Bran;

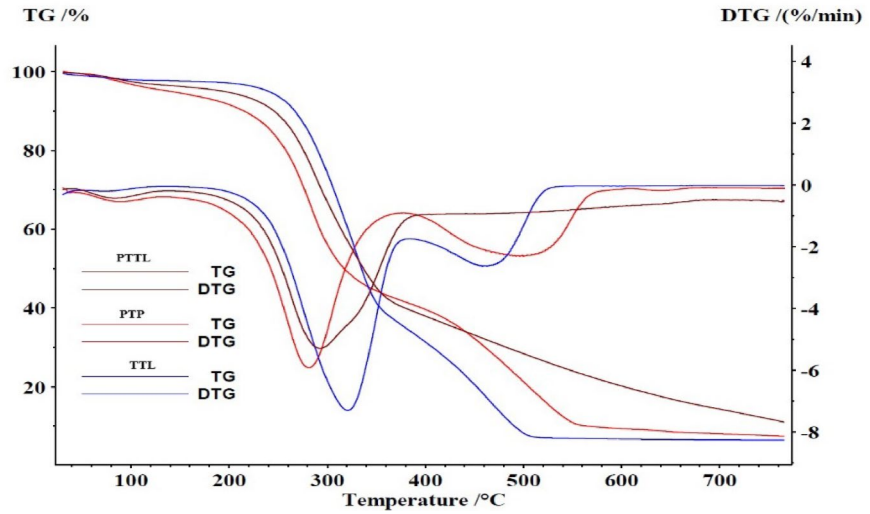

Fig. 5. TGA and DTG curve of PTP, PTTL and TTL.

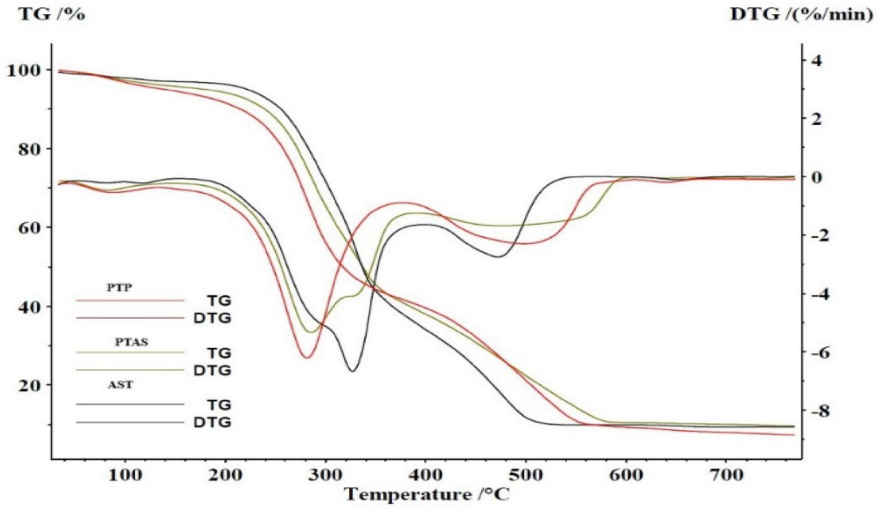

Fig. 6. TGA and DTG curve of PTP, PTAS and AST.

TLAS= Triticale + *Fraxinus excelsior***;** TLWH = Triticale + Wheat Bran**;**TTL = Triticale**;** WHAS = Wheat Bran + *Fraxinus excelsior* andWHB = Wheat Bran

The drying phase in thermogravimetric analysis (TGA) typically involves moisture reduction as the sample is heated within the temperature range of approximately 100–200 °C. This phase is crucial for evaluating lignocellulosic biomass samples as it reflects the sample's inherent moisture content and loosely bound water[44]. In the thermogravimetric profiles of the analyzed samples, an initial weight loss below 200 °C corresponds to moisture evaporation. Monitoring this drying phase, particularly in samples with high cellulose or hemicellulose content, provides insights into the moisture interaction with various lignocellulosic components.

Wheat bran (WHB), containing 56.79% hemicellulose and a relatively low cellulose content of 4.02%, exhibited its drying temperature onset at approximately 269.4 °C, with a distinct DTG peak at 300.3 °C as shown in Fig. 8, indicating hemicellulose decomposition. This observation aligns with Quan et al.[45]who reported that hemicellulose decomposes predominantly within the 210–370 °C range due to its amorphous structure, which facilitates moisture release and accelerates the drying process. Liu et al.[46] further investigated biomass thermal degradation and found that the mass loss temperature ranges are 200–327 °C for hemicellulose, 327–450 °C for cellulose, and 200–550 °C for lignin. These findings corroborate the thermal behaviours observed in this study.

For potato peel (PTP), the drying phase is influenced by its specific lignocellulosic composition, comprising 41.59% cellulose, 7.33% hemicellulose, and 7.53% lignin (refer to Table 11). Cellulose, as a crystalline polymer with low hygroscopicity, absorbs minimal moisture, facilitating the rapid release of water during heating[47]. This property, combined with PTP's high cellulose content, contributes to a faster drying phase than materials

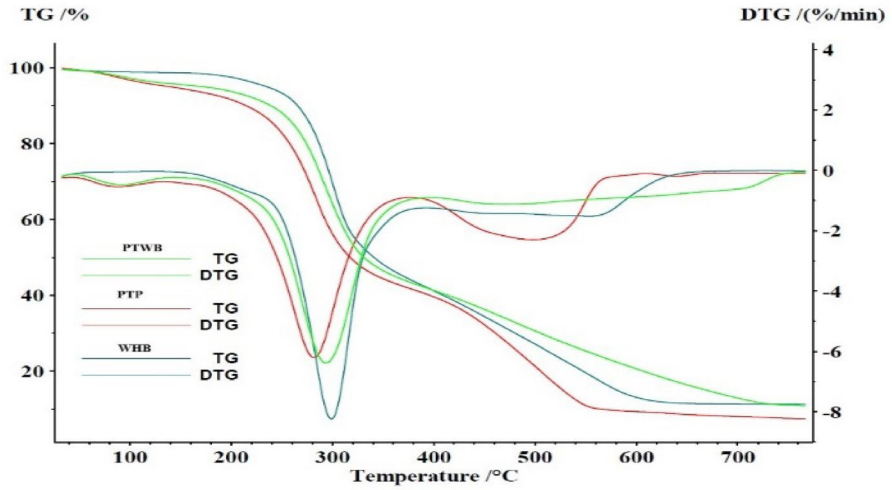

Fig. 7. TGA and DTG curve of PTWH, PTP and WHB.

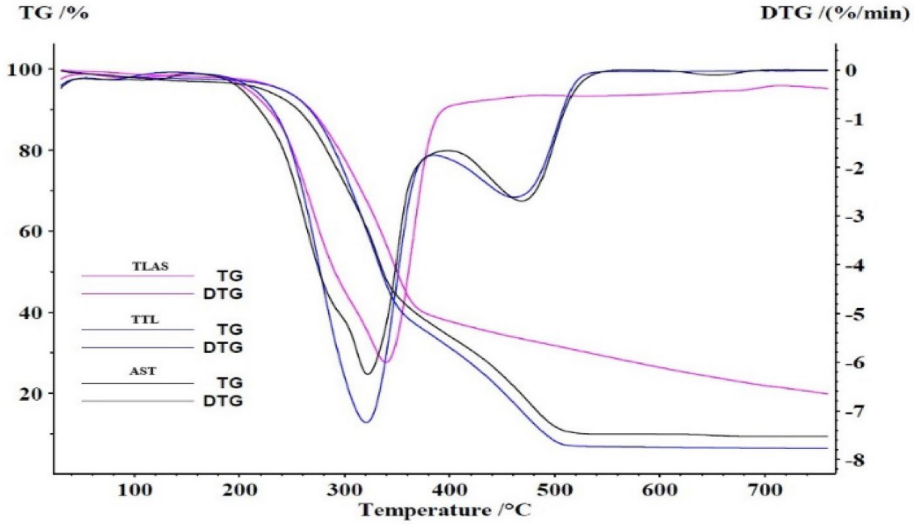

Fig. 8. TGA and DTG curve of TLAS, TTL and AST.

rich in hemicellulose. The significant initial weight loss observed in the TGA profile corresponds to cellulose's characteristic behaviour, where moisture is efficiently expelled with minimal retention.

PTP's low hemicellulose content further limits its capacity to retain moisture, resulting in a shorter drying period. In contrast, samples like Wheat Bran (WHB), with 56.79% hemicellulose, exhibit an extended drying phase due to hemicellulose's higher water-retaining properties. Mixtures of samples show different properties compared to pure samples. The potato peel and wheat bran mixture (PTWH), with substantial hemicellulose content derived from wheat bran, demonstrates the longest drying phase among the samples. Conversely, the potato peel and *Fraxinus excelsior* mixture (PTAS), containing only a small hemicellulose contribution from *Fraxinus excelsior* (AST), dries significantly faster. The drying duration across the samples follows the sequence Potato peel + Wheat Bran (PTWH) > Potato peel + Triticale (PTTL) > Potato peel and *Fraxinus excelsior* (PTAS), reflecting the direct relationship between drying time and hemicellulose content.

TTL (Triticale) features a balanced composition of 26.89% cellulose and 44.13% hemicellulose, resulting in a drying phase moderately influenced by both components. The cellulose content provides thermal stability, while the hemicellulose contributes to increased moisture retention. This balance is evident in the TGA profiles of mixed samples of potato peel and triticale (PTTL), and triticale and wheat bran (TLWH), which demonstrate extended drying phases compared to cellulose-dominated samples (wood residues), with onset temperatures of approximately 246.9 °C and 234.3 °C, as shown in Figs. 5 and 9, respectively. The drying trend corresponds to TTL's balanced lignocellulosic profile pure samples, resulting in a drying rate between rapid drying from the AST samples and gradual from WHB samples.

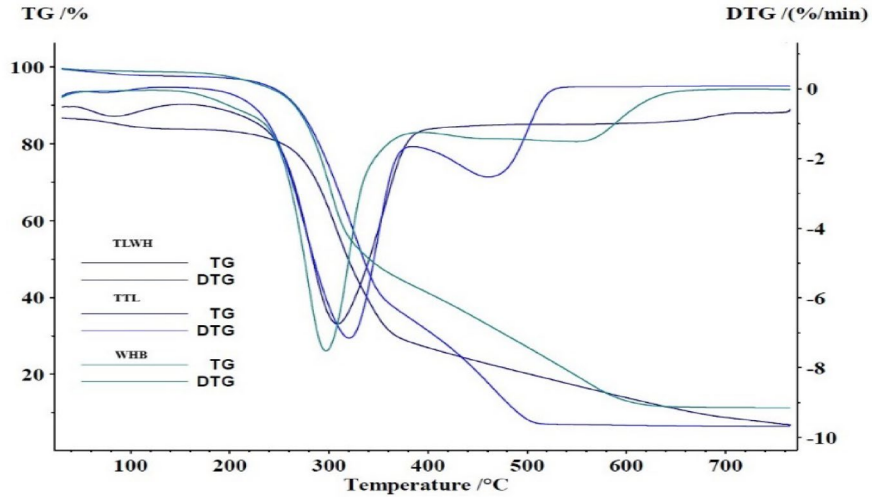

Fig. 9. TGA and DTG curve of TLWH, TTL and WHB.

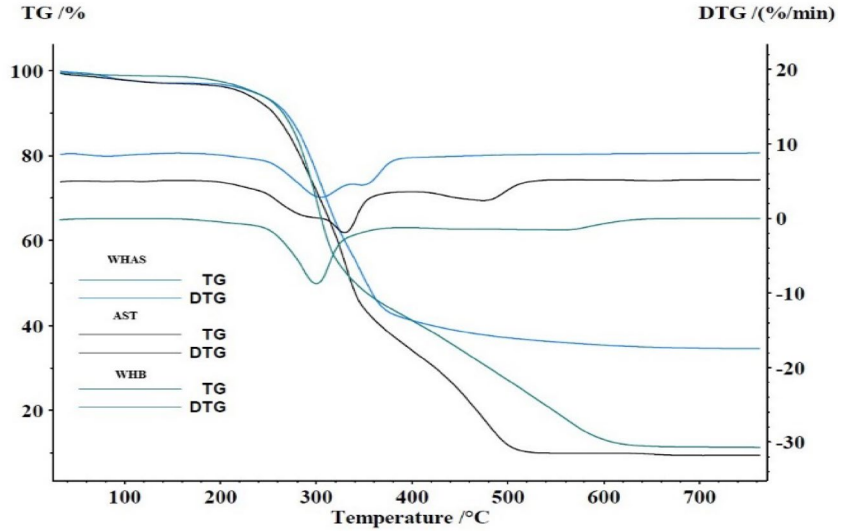

Fig. 10. TGA and DTG curve of WHAS, AST and WHB.

Fraxinus excelsior (AST) contains a high cellulose content (46.76%) alongside a significant hemicellulose proportion (28.33%), which retains bound water and requires energy to break the hydrogen bonds between water molecules and the matrix. As a result, AST demonstrates a drying phase at temperatures below 150 °C, consistent with the findings of Mishra and Vinu[48] where cellulose and hemicellulose contents were measured at 38.46% and 19.20%, respectively. The mixture of wheat bran and ash wood residues (WHAS), on the other hand, exhibits more distinct drying characteristics due to its higher hemicellulose content (56.79%), which enhances water retention.

In blends such as AST and its combinations, the influence of cellulose mitigates excessive moisture retention, creating a more balanced drying phase. For example, in the mix of samples triticale and *Fraxinus excelsior* (TLAS), the drying onset occurs at a higher temperature (276.6 °C), as shown in Fig. 8, indicating a controlled and gradual moisture release, influenced by the interplay of hemicellulose and cellulose.

Devolatilization primarily involves the thermal decomposition of volatile components, notably hemicellulose and cellulose, which exhibit distinct thermal stabilities due to their unique molecular structures. In this study, the *Fraxinus excelsior* (AST) sample comprises 46.76% cellulose, 28.33% hemicellulose, and 18.16% lignin, with significant decomposition occurring between approximately 270 °C and 471 °C, as shown in Fig. 4. This observation is consistent with work by Wang et al.[49] for pine wood sawdust. Broad peaks at 398.5 °C and 471.1 °C suggest the gradual breakdown of lignin, which imparts thermal stability across a wide temperature range[50].

For the potato peel sample (PTP), thermal degradation initiates at 245.1 °C, with prominent peaks at 281.7 °C, 377.2 °C, and 501.4 °C as shown in Fig. 4. The first peak corresponds to hemicellulose degradation, the second to cellulose decomposition, and the third to lignin breakdown[51]. The residual mass of 7.38% after thermal analysis

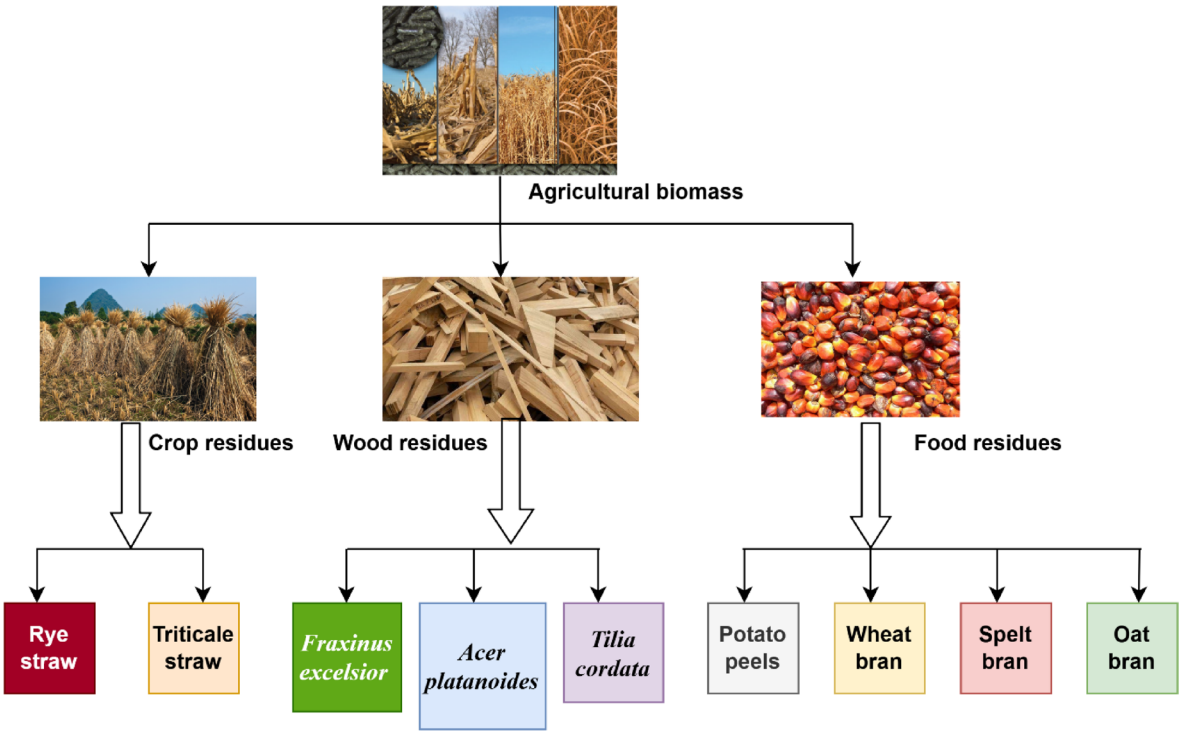

Fig. 11. Selected types of agricultural biomass.

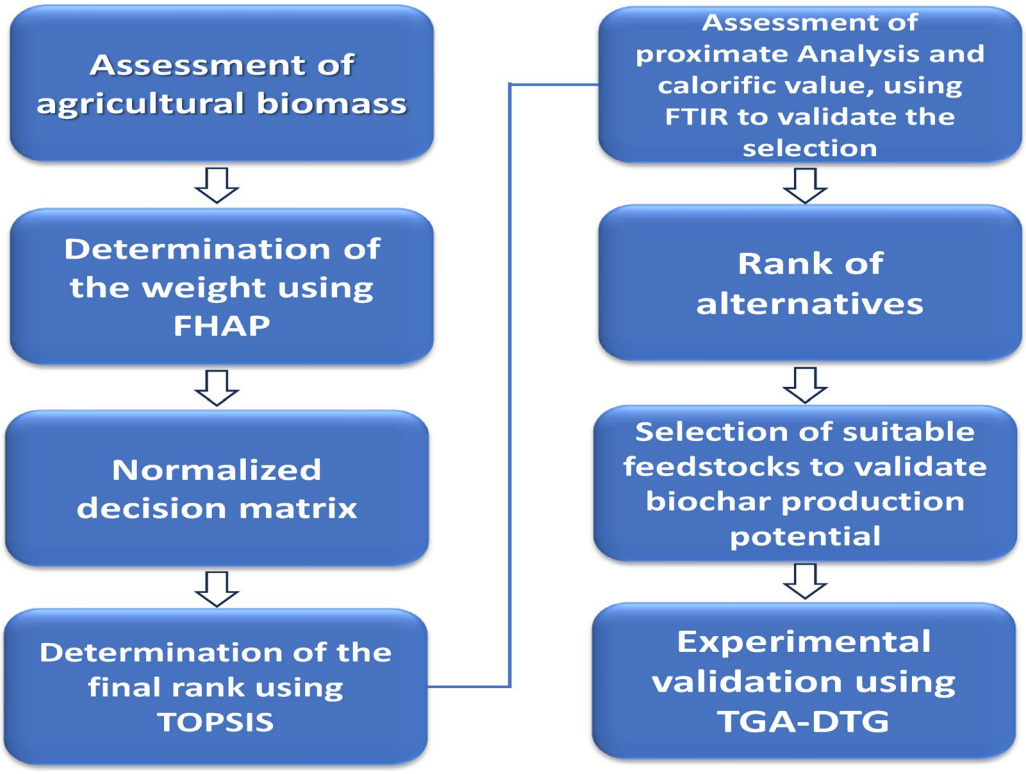

Fig. 12. Proposed integrated methodology.

Samples	Cellulose (%) (non-beneficial)	Hemicellulose (%) (non-beneficial)	Lignin (%) (beneficial)	Carbon (%) (beneficial)	Hydrogen (%) (non-beneficial)	Nitrogen (%) (beneficial)	Sulphur % (non-beneficial)	Oxygen (%) (non-beneficial)
Fraxinus excelsior	46.76	28.33	18.16	46.77	7.27	0.52	0.03	45.42
Acer platanoides	48.63	26.74	17.93	45.91	7.41	0.49	0.04	46.16
Tilia cordata	46.45	27.35	17.93	45.96	7.34	0.35	0.02	46.33
Spelt bran	4.46	53.68	6.57	41.80	7.88	2.31	0.21	47.21
Oat bran	3.77	53.03	4.70	41.24	8.14	2.10	0.21	47.31
Wheat bran	4.02	56.79	7.28	42.56	7.86	2.83	0.19	47.53
Potato peel	41.59	7.33	7.53	47.15	7.04	2.04	0.0775	44.95
Rye straw	16.38	41.12	12.68	42.00	7.00	0.66	0.16	48.92
Triticale	26.89	44.13	9.01	47.00	7.00	0.91	0.02	44.74

Table 11. Properties of the agricultural biomass materials of dry basis and decision matrix.

indicates moderate thermal stability, primarily attributed to the higher lignin content. The initial significant weight-loss peak at temperature 326.5 °C reflects hemicellulose devolatilization, while the subsequent peak at temperature 398.5 °C marks the onset of cellulose degradation.

In the wheat bran (WHB) sample, hemicellulose is notably high at 56.79%, while cellulose and lignin account for 4.02% and 7.27%, respectively, significantly influencing its devolatilization process. The TGA data for WHB shows an onset temperature of 269.4 °C and a peak at 300.3 °C. The high hemicellulose content likely explains the lower peak temperature, as hemicellulose thermally decomposes before cellulose. This is consistent with its amorphous and irregular structure, which features numerous branched units that require lower activation energy for decomposition[45]. The low cellulose content suggests that hemicellulose dominates the devolatilization process, particularly in the earlier stages.

For triticale (TTL), the composition includes 26.89% cellulose, 44.13% hemicellulose, and 9.06% lignin. TGA analysis indicates peaks at temperatures 320.9 °C and 458.0 °C as shown in Fig. 4, reflecting a balanced contribution from hemicellulose and cellulose during devolatilization. The initial peak at temperature 320.9 °C corresponds to hemicellulose degradation, while the second peak at 458.0 °C signifies a significant role of cellulose as shown in Fig. 4. The sharp and early DTG peak suggests a rapid breakdown of components driven by the higher proportion of hemicellulose, which decomposes faster than lignin[52].

In the potato peel and *Fraxinus excelsior* blend (PTAS), the devolatilization process starts at an onset temperature of 247.6 °C, with prominent decomposition peaks observed at 284.8 °C and 331.8 °C, as illustrated in Fig. 6. The crystalline structure of cellulose results in slower degradation compared to hemicellulose, producing a distinct DTG peak. This behavior is influenced by the combination of cellulose-rich *Fraxinus excelsior* (AST) and potato peel (PTP). The first peak at 284.8 °C corresponds to the degradation of hemicellulose, reflecting the significant hemicellulose content in PTP. The second peak at 331.8 °C indicates cellulose decomposition, attributed to the high cellulose content in AST and PTP, at 46.76% and 41.59%, respectively. The extended temperature range demonstrates a complex process where hemicellulose degrades first, followed by cellulose, with lignin from both materials contributing to the blend's thermal stability at elevated temperatures.

In the potato peel and triticale blend (PTTL), the devolatilization process begins at an onset temperature of 246.9 °C, with decomposition peaks occurring at 288.0 °C and 328.3 °C as shown in Fig. 5. The introduction of triticale (TTL), which contains 44.13% hemicellulose and 26.89% cellulose, influences the increase in the devolatilization at the beginning and on the secondary growth. The first peak at the beginning in 288.0 °C is associated with hemicellulose degradation, while the secondary growth at temperature 328.3 °C corresponds to cellulose decomposition, primarily contributed by potato peel (PTP) with a cellulose content of 41.59%. This sequential degradation pattern aligns with the characteristic decomposition temperatures of hemicellulose and cellulose. Additionally, the lignin present in both PTP and TTL enhances the thermal stability of the blend at higher temperatures, supporting a gradual and staged devolatilization process.

In the potato peel and wheat bran blend (PTWH), devolatilization begins at a slightly higher onset temperature of 256.8 °C, with a prominent increase at 293.8 °C, as illustrated in Fig. 7. The substantial hemicellulose content in wheat bran (56.79%) and its low cellulose content (4.02%) largely accounts for the distinct singular peak observed in the DTG curve. The rapid weight loss at 293.8 °C corresponds primarily to hemicellulose degradation, with minimal contribution from cellulose. The elevated onset temperature can be attributed to the stabilizing influence of lignin in wheat bran, which marginally prolongs thermal stability without significantly affecting the hemicellulose-dominated peak.

In the triticale and *Fraxinus excelsior* blend (TLAS), devolatilization commences at 276.6 °C, with a main increase at 345.6 °C, as depicted in Fig. 8. This blend combines TTL's moderate cellulose content (26.89%) and high hemicellulose content (44.13%) with AST's significant cellulose content (46.76%). The higher onset and peak temperatures reflect a stronger contribution from cellulose and the synergistic stabilizing effect of lignin from both materials. The peak at 345.6 °C represents cellulose degradation, which is more pronounced in this blend, highlighting the role of increased cellulose content in shifting devolatilization to higher temperatures.

For the triticale and wheat bran blend (TLWH), devolatilization starts at 234.3 °C, with a primary increase at 315.4 °C as shown in Fig. 9. Triticale's balanced cellulose (26.89%) and hemicellulose (44.13%) composition, combined with wheat bran's substantial hemicellulose content (56.79%) and minimal cellulose (4.02%), defines the thermal behaviour. The early onset temperature reflects the lower thermal stability of hemicellulose, while the peak at 315.4 °C results from the combined degradation of hemicellulose and some cellulose. The influence of triticale's cellulose content slightly elevates the peak temperature compared to pure wheat bran, indicating a complex interaction of these components.

In the wheat bran and *Fraxinus excelsior* blend (WHAS), devolatilization begins at 263.6 °C, with peaks at 304.5 °C and 351.5 °C, as depicted in Fig. 10. The high cellulose content in AST (46.76%) and the significant hemicellulose level in wheat bran (56.79%) drive the thermal profile. The initial peak at 304.5 °C is attributed to hemicellulose degradation, while the secondary peak at 351.5 °C corresponds to cellulose breakdown from AST. The dual-peak pattern highlights the sequential decomposition of hemicellulose and cellulose. Lignin's presence enhances thermal stability throughout the temperature range, contributing to prolonged devolatilization, as evident from the staggered peaks and residual mass at higher temperatures.

The thermogravimetric analysis (TGA) results for the tested samples, which are potato peel, *Fraxinus excelsior*, triticale, and wheat bran, reveal degradation trends that closely align with their lignocellulosic compositions. Typically, char generation occurs after the primary devolatilization phases, generally at temperatures exceeding 400 °C, once most volatile compounds have been released. These findings are consistent with prior studies on biomass, such as coffee husk, where Nam et al.[53] observed the third phase of weight loss at elevated temperatures above 400 °C, characterized by intermediate decomposition and the slower thermal degradation of lignin. Similarly, Linh et al.[54] reported that char formation in macadamia nutshells begins around 450 °C. Lignin's complex, cross-linked structure, which decomposes over a broad temperature range (200–700 °C), is instrumental in char production, contributing to enhanced thermal stability and higher char yields.

The AST sample, with a lignin content of 18.16%, demonstrates significant stability beyond the degradation phases of cellulose and hemicellulose. This stability results in a notable residual mass and robust char formation at elevated temperatures, persisting up to 769.6 °C. The TGA profiles highlight variations in lignocellulosic composition across the samples. AST and TTL show higher cellulose-to-lignin ratios, at 47.44:18.04% and 27.13:9.9%, respectively as shown in Fig. 8; Table 11. Biomass blends rich in both cellulose and lignin, such as TLAS, exhibit favourable properties for biochar production. TLAS achieves the highest residual mass at 760.5 °C (29.26%) as shown in Fig. 7, primarily due to AST's substantial lignin content.

In the wheat bran and *Fraxinus excelsior* blend (WHAS), the high lignin content from AST significantly enhances char stability at elevated temperatures. It substantially increases the residual mass after thermal degradation. Lignin's thermal resilience compensates for WHB's lower lignin content (7.27%) and high hemicellulose proportion (56.79%), which would otherwise lead to rapid decomposition. This blend, through the lignin-rich composition of AST, allows for higher and more consistent char formation than other blends. The properties of lignin-rich biomass, such as that found in AST, make it particularly well-suited for biochar applications, offering improved porosity, structural integrity, and practical benefits for soil enhancement and carbon sequestration.

Balancing biomass parameters for energy, soil amendment, and water treatment applications

The selection of agricultural biomass for biochar production is a complex process that requires balancing beneficial and non-beneficial parameters, which significantly influence the final biochar's quality and its application in different fields. Beneficial parameters such as lignin, carbon, and nitrogen are crucial for the effectiveness of biochar in energy density, water treatment, and soil amendment. Lignin, with its high carbon content and thermal stability, enhances the structural integrity and porosity of biochar. This is particularly important for biochar's role in soil amendment, as it improves soil structure and promotes carbon sequestration[9]. Lignin also plays a vital role in water treatment by enhancing the biochar's adsorption properties, making it effective for contaminant removal[11]. Furthermore, lignin's thermal stability helps in energy applications, where higher lignin content increases the biochar's calorific value, improving its energy density[7].

Carbon content is another critical beneficial parameter. High carbon levels are directly linked to biochar's energy potential, as carbon is the primary element responsible for energy release during combustion. This makes biomass with high carbon content especially useful for energy generation, as it maximizes the calorific value of the resulting biochar[5]. Additionally, nitrogen content, although beneficial for soil amendment by improving soil fertility, can sometimes present challenges, especially when high levels of nitrogen lead to reduced biochar stability and increased ammonia emissions. Despite this, nitrogen-enriched biochar remains valuable for improving soil quality and fostering better crop yields in agricultural systems[9].

On the other hand, non-beneficial parameters such as cellulose, hemicellulose, sulfur, and oxygen need to be carefully controlled when selecting biomass for biochar production. Cellulose and hemicellulose are polysaccharides that are more suited for bio-oil production during pyrolysis rather than biochar. These components are less desirable in biochar as they are less stable, decompose at lower temperatures, and result in a biochar product with lower carbon content. This reduction in carbon affects the energy density of the biochar, making it less effective for energy generation[31]. Sulphur content, while sometimes useful in treating specific soils (e.g., arid soils), is generally considered non-beneficial in biochar production. High sulphur levels can lower biochar's pH, reducing its stability and making it less suitable for both energy and water treatment applications[11]. Similarly, high oxygen content during pyrolysis can lead to a decrease in carbon content, lowering the biochar's calorific value and its overall effectiveness in energy applications[7].

The final biochar product's suitability for various applications depends on the careful optimization of these parameters. In energy generation, the goal is to maximize carbon content, with high lignin being beneficial

to enhance thermal stability and increase calorific value. For water treatment, biochar's porosity and surface area, enhanced by lignin and nitrogen content, make it effective in adsorbing contaminants. In soil amendment, nitrogen is particularly important for improving soil fertility, while high lignin content improves soil structure and water retention. Minimizing non-beneficial parameters like cellulose, hemicellulose, and sulphur ensures that the biochar is stable, efficient, and functional for its intended purpose. Thus, the selection process involves a balance of these beneficial and non-beneficial factors to optimize biochar production for specific end-use applications[4].

Methods

Materials preparation

The agricultural biomass samples used in this research were collected from Bialystok, Poland. They were pulverized and screened to a particle size of 1 mm. To reduce moisture content, the samples were initially dried under direct sunlight for two weeks, followed by oven drying at 100 °C for one hour. This process was conducted in a closed chamber using a high-temperature furnace. The samples were selected due to their abundant availability and represented three categories of agricultural biomass: wood residue, crop residue, and food waste, as illustrated in Fig. 11. For experimental validation using TGA-DTG, the top-ranked agricultural biomass material was chosen from both the wood and crop residue categories, while two top-ranked biomass materials were selected from the food waste category.

Analysis of lignocellulosic composition in agricultural biomass samples

The lignocellulosic composition, including lignin, hemicellulose and cellulose, was determined using a modified method described by Bamisaye et al.[55]. A 1 g sample of dried material (a) was combined with 150 mL of demineralized water and heated in an oil bath at 100 °C for 1 h. After heating, the mixture was filtered, the filtrate discarded, and the residue washed with 300 mL of hot demineralized water. The washed residue was subsequently dried in an oven with periodic weighing until a constant weight was achieved (b). The dried residue was then treated with 150 mL of 1 N H_2SO_4 and heated at 100 °C in an oil bath for 1 h. The mixture was filtered, and the solid residue was washed with 300 mL of demineralized water before being dried to a constant weight (c). Next, the residue was soaked in 10 mL of 72% H_2SO_4 at room temperature for 4 h. Following this, 150 mL of 1 N H_2SO_4 was added, and the mixture was refluxed in an oil bath for 1 h. The solid was washed with 400 mL of demineralized water, dried in an oven at 105 °C, and weighed until a constant weight was noted (d). Finally, the solid was ashed, and the remaining material was weighed (e). The percentages of hemicellulose, cellulose, and lignin were calculated based on the recorded weights.

$$\%\, hemicellulose = \frac{(c-b)}{a} \times 100\% \tag{1}$$

$$\%\, cellulose = \frac{(d-c)}{a} \times 100\% \tag{2}$$

$$\%\, lignin = \frac{(e-d)}{a} \times 100\% \tag{3}$$

Proximate analysis of agricultural biomass samples

The moisture content (per PN-EN ISO 18134[56]), volatile matter content (per PN-EN ISO 18123[57]), and ash content (per PN-EN ISO 18122[58]) of agricultural biomass feedstocks were analyzed using the TGA-701 analyzer from LECO, while the fixed carbon content was calculated by difference.

$$FC = 100 - (MC - AS - VM) \tag{4}$$

In the agricultural biomass, FC, MC, AS, and VM represent the fixed carbon, moisture content, ash content, and volatile matter content, respectively, with all values measured on a consistent analytical basis.

Ultimate analysis of agricultural biomass samples

The carbon, nitrogen, hydrogen, and sulphur content were analyzed using the LECO CHN628 analyzer, following the standards PN-EN 15104[59], PN-EN ISO 16948[60], and PN-EN ISO 16994[61], respectively. This device employs combustion techniques, providing results in weight percentages or parts per million (ppm). The analyzer was operated using software running on the Windows operating system, with external computer managing system control and data processing.

Calorific values of agricultural biomass samples

The higher heating value (HHV) of the raw materials was determined following the PN-ISO 1928[62] standard. The HHV measurement was conducted using the KL-12Mn calorimeter, manufactured by Precyzja-Bit (Poland). This process involved the complete combustion of the fuel sample in a calorimetric bomb under an oxygen atmosphere at elevated pressure, with temperature increases recorded as an indicator of the thermal effect of combustion. The lower heating value (LHV) was then calculated accordingly.

$$LHV = \frac{100-w}{100}.HHV - \frac{\gamma .w}{1000}\left(MJ.kg^{-1}\right) \tag{5}$$

where w—moisture content (%); γ—heat of vaporization of water at 20 °C, corresponding to the content of 1% water in the fuel ($\gamma = 24.55$ kJ · kg^{-1}) (kJ · kg^{-1}).

Thermogravimetric analyses

A thermogravimetric analysis (TGA) system (NETZSCH, Libra 209 F1) was employed to assess the maximum conversion rates and degradation temperatures of individual biomass samples and their mixture prior to pyrolysis experiments. Approximately 12 ± 0.1 mg of biomass was precisely weighed using a sensitive balance (METTLER TOLEDO, XS204) and placed in ceramic crucibles. The samples were positioned on a high-sensitivity calculated differential thermal analysis (c-DTA*) platform, equipped with a SiO_2-coated sample carrier. The analysis was conducted under a continuous flow of high-purity nitrogen gas (99.999%) at a rate of 20 mL·min^{-1}. The samples were heated from 25 °C to 800 °C at a consistent rate of 10 K·min^{1}. The derivative thermogravimetric (DTG) curves were derived from the TGA curves as described by Ekici et al.[63].

FT-IR analysis

FTIR ATR is Fourier Transform Infrared Spectroscopy, Attenuated Total Reflectance technique. The samples tested in powdered form were ground in an agate mortar. Then a small amount of the sample was applied to the ATR crystal and the measurement was performed. The FTIR infrared spectra was recorded using the ATR (Attenuated Total Reflectance) technique in the wavenumber range of 2000 cm^{-1}- 600 cm^{-1}. The number of measurement scans was 32. The measurement resolution was 1 cm^{-1}. The measurements were performed on a Bruker Alfa spectrophotometer using OPUS software.

Methodology in multi-criteria decision-making (MCDM) processes

Attributing weights or scores are crucial in multi-criteria decision-making (MCDM) processes. Although criterion values indicate the attributes, characteristics, and results of alternatives, attribute weights assist in evaluating the importance of particular features within a specific process[64]. The organized analysis for sustainable biochar production includes the subsequent steps:

- Assessment of agricultural biomass and decision matrix (Table 11).
- Determination of the criteria weights using FAHP.
- Normalized decision matrix.
- Determination of the final rank using TOPSIS.
- Assessment of proximate analysis and calorific value, along with FT-IR, to validate the selection.
- Ranking of alternatives.
- Selecting suitable feedstocks to validate biochar production potential.
- Experimental validation using TGA-DTG.

Figure 12 presents the block diagram of the proposed integrated methodology in this study.

FAHP method

The Analytic Hierarchy Process (AHP) is a widely used decision-making technique. An advanced variant, Fuzzy AHP (FAHP), integrates AHP with fuzzy logic, first introduced by Zadeh, to handle linguistic expressions in decision analysis[65].

The process for calculating criterion weights is outlined below:

Step 1: Define the complex material selection problem using a hierarchical structure with three levels: the main objective, criteria, and alternatives.

Step 2: Construct the pairwise comparison matrix using triangular fuzzy numbers to generate a crisp pairwise comparison matrix (Ã). Table 12 illustrates the membership functions for linguistic terms on a nine-point scale. For a triangular fuzzy number (F), the membership function $\mu_{\widehat{F}}(x)$ is expressed using the following equation. Table 12

Intensity of importance	Definition	TFN (L, M, U)	Reciprocal of TFN (1/U, 1/M, 1/L)
1	Equal Importance	(1,1,1)	(1,1,1)
2	Weak or slight	(1,2,3)	(0.33,0.5,1)
3	Moderate Importance	(2,3,4)	(0.25,0.33,0.5)
4	Moderate Plus	(3,4,5)	(0.2,0.25,0.33)
5	Strong Importance	(4,5,6)	(0.16,0.2,0.25)
6	Strong Plus	(5,6,7)	(0.14,0.16,0.2)
7	Very Strong	(6,7,8)	(0.12,0.14,0.16)
8	Very, Very Strong	(7,8,9)	(0.11,0.12,0.14)
9	Extreme Importance	(8,9,10)	(0.10,0.11,0.12)

Table 12. Membership function of fuzzy numbers. Abbreviation: tfn = triangular fuzzy numbers; L, M and u = the possibles values of the membership function.

Number of criteria (n)	RCI
1	0
2	0
3	0.58
4	0.90
5	1.12
6	1.24
7	1.32
8	1.41
9	1.45
10	1.49

Table 13. Average RCI values.

$$\mu_{\widehat{F}}(x) = \begin{cases} {}^{(x-l)}_{(m-l)}, \; l \le x \le m \\ {}^{(u-x)}_{(u-m)}, \; m \le x \le u \\ 0, \; l \ge x \ge u \end{cases}, \text{ where l, m, and u are the possible values of the membership function}$$

$$\widetilde{\mathrm{A}} = \begin{bmatrix} 1 & \widehat{a}_{12} & \cdots & \widehat{a}_{1n} \\ \frac{1}{\widehat{a}_{12}} & 1 & \cdots & \widehat{a}_{2n} \\ \vdots & \vdots & \ddots & \vdots \\ \frac{1}{\widehat{a}_{1n}} & \frac{1}{\widehat{a}_{2n}} & \cdots & 1 \end{bmatrix}, \; \widehat{a}_{ij} = (1,1,1), \; \widehat{a}_{ji} = \frac{1}{\widehat{a}_{ij}} \tag{6}$$

Suppose $\widehat{a}_{12} = (l_1, m_1, u_1)$, then

$$\frac{1}{\widehat{a}_{12}} = \left(\frac{1}{u_1}, \frac{1}{m_1}, \frac{1}{l_1}\right) \tag{7}$$

Step 3: Determination of fuzzy weights of each criterion $\widehat{w}_i$

Were,

$$\widehat{w}_i = \frac{\widehat{r}_i}{(\widehat{r}_1 \oplus \widehat{r}_2 \oplus \ldots . \oplus \widehat{r}_i \oplus \ldots \ldots \ldots \widehat{r}_n} \tag{8}$$

$$\widehat{r}_i = (\widehat{a}_{i1} \oplus \widehat{a}_{i2} \oplus .. \oplus \widehat{a}_{ij} \oplus .. \oplus \widehat{a}_{in})^{\frac{1}{n}}$$

Step 4: Defuzzification of fuzzy output using the formula.

$$\frac{1}{3}(1 + u + m) \tag{9}$$

Step 5: Assess the importance of factors by calculating the Eigenvectors associated with the largest Eigenvalues from the comparisons.

Step 6: Verify the consistency of the evaluations by using the Consistency Index (CI) and the Consistency Ratio (CR).

$$CI = \frac{\lambda_{max} - n}{n - 1} \tag{10}$$

The consistency ratio (CR) is calculated as the ratio of the Eigen value λ_{max}, derived from the pair-wise comparison matrix, to the total number of elements being evaluated, denoted as n.

$$CR = \frac{CI}{RCI} \tag{11}$$

The Random Consistency Index (RCI), as presented in Table 13, is applied here. Typically, a CR value below 0.1 is considered acceptable. If the CR exceeds this threshold, the pairwise comparisons should be reassessed to address any inconsistencies.

TOPSIS method

The TOPSIS method is used to evaluate rankings after determining the weights for each criterion. Developed by Hwang and Yoon[66] TOPSIS offers an efficient way to generate results quickly, and it is one of the most reliable techniques for comparing different alternatives. This method focuses on calculating the distances between the ideal and non-ideal solutions. Criteria that benefit the system are maximized, while those that hinder it are

minimized, leading to the optimal result, as shown in Table 11. This method is based on mathematical concepts, and it is effective for comparing multiple options. Additionally, its flexibility allows it to be applied to various scenarios, particularly in engineering problems[67]. The weights derived from the AHP method are integrated into the TOPSIS process to rank alternatives based on the influence of each criterion on the overall system or model. This enhances system performance by identifying the best options and prioritizing key parameters.

The combined modelling process follows these steps:.

Step 1: Experts provide input to create a matrix using linguistic values to assess the significance of each criterion based on system outcomes. The criteria are scored on a scale from 1 to 9 as shown in Table 12, with values representing different levels of importance, from "equal importance" to "extreme importance." Eqs. (12)–(20) from Ahmad et al.[67] were applied.

Step 2: The linguistic values from the experts are converted into precise numerical estimates.

$$X_{abN} = (labN)\ Where,\ a = 1,\ 2,\ 3, \ldots \ldots\ m; b = 1,\ 2,\ 3, \ldots \ldots, n,\ where,$$

$$a = \min\{l_{abN}\},\ b = \frac{1}{N}\sum_{N-1}^{N} P_{abN},\ c = \max(u_{abN}) \tag{12}$$

Step 3: Estimating the result evaluations by combining the weights.

$$B = [P_{IJ}]_{mxn} \tag{13}$$

$$Here,\ i = 1,\ 2,\ 3,\ 4 \ldots,\ m; j = 1,\ 2,\ 3,\ 4 \ldots ., n$$

$$P_{ij} = \left(\frac{a_{ij}}{c_j^*}\right);\ c_j^* = maxc_{ij} \tag{14}$$

$$P_{ij} = \left(\frac{a_j^-}{c_{ij}}\right);\ a_j^* = mina_{ij} \tag{15}$$

Step 4: Normalizing the general resultant matrix.

$$V = [v_{ij}]_{\ mxn}\ where,\ i = 1,\ 2,\ 3,\ \ldots,\ m; j = 1,\ 2,\ 3,\ \ldots,\ n \ldots \ldots\ 7$$

$$Here,\ v_{ij} = p_{ij}(\times)\, w_j \tag{16}$$

Step 5: Calculating the homogenous weightage attained matrix.

$$A^+ = \left\{v_1^+, \ldots .., v_n^+\right\} \tag{17}$$

$$where,\ v_j^+ = \left\{max(v_{ij})\ IF \in\ J; minv_{ij}IF_j \in\ J'\right\},\ j = 1,\ 2,\ 3,\ \ldots .n \ldots \ldots\ 17$$

$$A^- = \left\{v_1^-, \ldots \ldots, v_n^+\right\}$$

$$where,\ v_j^- = \left\{max(v_{ij})\ IF \in\ J; minv_{ij}IF_j \in\ J'\right\},\ j = 1,\ 2,\ 3,\ \ldots .n \ldots \ldots\ 18$$

Step 6: Furnishing the optimum results, which might be either positive or negative.

$$d_i^+ = \left\{\sum_{j=1}^{n}(v_{ij} - v_{ij}^+)\right\}^{\frac{1}{2}}; i = 1,\ 2,\ \ldots,\ m \tag{18}$$

$$d_i^- = \left\{\sum_{j=1}^{n}(v_{ij} - v_{ij}^-)\right\}^{\frac{1}{2}}; i = 1,\ 2,\ \ldots,\ m \tag{19}$$

Step 7: Analyzing the differences between the actual data collected and the ideal, including both positive and negative variations.

$$CC_i = \frac{d_i^-}{d_i^- + d_i^+}; i = 1,\ 2,\ \ldots \ldots\ n \tag{20}$$

Step 8: The final value of the closeness coefficient (CC) is approximated, and the ranking is determined. The value with the highest CC receives the top rank, while the rank decreases as the CC value decreases.

Conclusions

This research highlights the significant role of agricultural biomass in sustainable biochar production. The AHP-TOPSIS method proved effective in identifying optimal biomass feedstocks, with key factors such as lignin content, carbon concentration, and nitrogen content being crucial in determining biochar quality. The selection of Fraxinus excelsior, potato peels, and wheat bran, along with triticale straw, offers practical implications for eco-friendly waste utilization, contributing to resource efficiency in agriculture.

The thermogravimetric analysis further elucidates the thermal properties of the chosen agricultural biomass feedstocks, highlighting their potential for biochar production. The complex, cross-linked structure of lignin

plays a critical role in char production by enhancing thermal stability and boosting char yields. Both *Fraxinus excelsior* and triticale demonstrate higher cellulose-to-lignin ratios, with values of 47.44:18.04% and 27.13:9.9%, respectively. Biomass blends rich in both cellulose and lignin, such as *Fraxinus excelsior* and triticale (TLAS), exhibit favourable properties for biochar production. The combination of *Fraxinus excelsior* and triticale reaches the highest residual mass at 760.5 °C (29.26%), primarily due to the substantial lignin content in AST.

Additionally, this study contributes to the broader discussion on sustainable agricultural practices by advocating for the efficient use of agricultural waste, enhancing resource efficiency. The integration of advanced analytical techniques including FTIR and proximate analysis with decision-making models establishes a strong foundation for future research aimed at improving biochar production methods. Ultimately, this study paves the way for further exploration into the relationship between biomass characteristics and biochar quality and techno-economic analysis, offering valuable insights for researchers, practitioners, and policymakers focused on advancing sustainable agriculture and environmental responsibility.

Data availability

The data generated or analyzed during this study are included in this published article. The datasets used and/or analyzed during the current study are available from the corresponding author on reasonable request.

Received: 16 May 2025; Accepted: 9 July 2025
Published online: 09 August 2025

References

1. Roszkowska, S. & Szubska-Włodarczyk, N. What are the barriers to agricultural biomass market development? The case of Poland. *Environ. Syst. Decis.* **42**, 75–84 (2022).
2. European Commission. Analysis of options beyond 20% GHG emission reductions: member state results. Commission Staff Working Paper. (2012).
3. Panoutsou, C. The role of sustainable biomass in the heat market sector for EU27. *Wiley Interdiscip Rev. Energy Environ.* **5** (4), 430–450 (2016).
4. Mandova, H. et al. Possibilities for CO_2 emission reduction using biomass in European integrated steel plants. *Biomass Bioenerg.* **115**, 231–243 (2018).
5. Giuntoli, J. et al. Climate change impacts power generation from residual biomass. *Biomass Bioenerg.* **89**, 146–158 (2016).
6. Janiszewska, D. & Ossowska, L. The role of agricultural biomass as a renewable energy source in European union countries. *Energies* **15**, 1–14 (2022).
7. Ige, A. R. & Łaska, G. Production of antioxidant additives and Biochar pellets from the Co-pyrolysis of agricultural biomass: A review. *Renew. Sustain. Energy Rev.* **208**, 1–17 (2025).
8. Camia, A. et al. *Biomass Production, Supply, Uses and Flows in the European Union: First Results from an Integrated Assessment. EUR - Scientific and Technical Research Reports*JRC109869 (Publications Office of the European Union, 2018).
9. Rangabhashiyam, S. & Balasubramanian, P. The potential of lignocellulosic biomass precursors for Biochar production: performance, mechanism and wastewater application — a review. *Ind. Crops Prod.* **128**, 405–423 (2018).
10. Amalina, F. et al. Water hyacinth (Eichhornia crassipes) for organic contaminants removal in water – A review. *J. Hazard. Mater. Adv.* **7**, 1–10 (2022a).
11. Patel, M. R. & Panwar, N. L. Biochar from agricultural crop residues: environmental, production, and life cycle assessment overview. *Resour. Cons Recy Adv.* **19**, 1–16 (2023).
12. Madhu, P. et al. Selection of biomass materials for bio-oil yield: a hybrid multicriteria decision making approach. *Clean. Techn Environ. Policy*. **20**, 1377–1384 (2018).
13. Dhanalakshmi, C. S. et al. A comprehensive MCDM-based approach using TOPSIS and EDAS as an auxiliary tool for pyrolysis material selection and its application. *Biomass Conv Bioref.* **12**, 5845–5860 (2022).
14. Triantaphyllou, E. et al. Determining the most important criteria in maintenance decision making. *J. Qual. Maint Eng.* **3**, 16–2822 (1997).
15. Chan, F. T. S. et al. Global supplier selection: a fuzzy-AHP approach. *Int. J. Prod. Res.* **46**, 3825–3857 (2008).
16. Zadeh, L. A. Fuzzy sets. *Inf. Control*. **8**, 338–353 (1965).
17. Hanine, M. et al. Application of an integrated multi-criteria decision making AHP-TOPSIS methodology for ETL software selection. *SpringerPlus* **263**, 1–16 (2016).
18. Sivalingam, C. & Subramaniam, S. K. Cobot selection using hybrid AHP-TOPSIS based multi-criteria decision-making technique for fuel filter assembly process. *Heliyon* **10**, 1–11 (2024).
19. Amiri, A. A. et al. A strategic multi-criteria decision-making framework for renewable energy source selection in Saudi Arabia using AHP-TOPSIS. *Renew. Energy*. **236**, 1–14 (2024).
20. Zoma, F. & Sawadogo, M. A multicriteria approach for biomass availability assessment and selection for energy production in Burkina faso: A hybrid AHP-TOPSIS approach. *Heliyon-* **9** (10), 1–17 (2023).
21. Xu, S. et al. Effect of biomass type and pyrolysis temperature on nitrogen in biochar, and the comparison with hydrochar. *Fuel* **291**, 1–11 (2021).
22. Leng, L. et al. Nitrogen containing functional groups of biochar: an overview. *Bioresour Technol.* **298**, 1–52 (2020).
23. Rambhatla, N. et al. Biomass pyrolysis for Biochar production: study of kinetics parameters and effect of temperature on Biochar yield and its physicochemical properties. *Results Eng.* **25**, 1–12 (2025).
24. Mukherjee, A. et al. Synthesis of Biochar from lignocellulosic biomass for diverse industrial applications and energy harvesting: effects of pyrolysis conditions on the physicochemical properties of Biochar. *Front. Mater.* **9**, 1–10 (2022).
25. Vilas-Boas, A. C. M. et al. Methodologies for bio-oil characterization from biomass pyrolysis: A review focused on GC-MS. *J. Anal. Appl. Pyrol.* **185**, 1–20 (2025).
26. Zailani, R., Ghafar, H. & So'aib, M. S. Effect of oxygen on Biochar yield and properties. *Int. J. Mech. Aero Indust Mechatron. Eng.* **7**, 1–5 (2013).
27. Al-Rabaiai, H. et al. Biochar pH reduction using elemental sulfur and biological activation using compost or vermicompost. *Bioresour Technol.* **40**, 1–10 (2024).
28. Weber, K. & Quicker, P. Properties of Biochar. *Fuel* **217**, 240–261 (2018).
29. Dong, J. et al. Effect of operating parameters and moisture content on municipal solid waste pyrolysis and gasification. *Energy Fuels*. **30**, 3994–4001 (2016).
30. Yao, X. et al. A comprehensive study on the influence of operating parameters on agglomeration of ashes during biomass gasification in a laboratory-scale gasification system. *Fuel* **276**, 1–12 (2020).

31. Wiwart, M. et al. Spelt (Triticum spelta) and emmer (T. dicoccon) chaff used as a renewable source of energy. *BioResources* **12**, 3744–3750 (2017).
32. Panepinto, D., Viggiano, F. & Genon, G. Energy production from biomass and its relevance to urban planning and compatibility assessment: two applicative cases in Italy. *Clean. Technol. Environ. Policy*. **17**, 1429–1442 (2014).
33. Oh, S. Y. et al. FTIR analysis of cellulose treated with sodium hydroxide and carbon dioxide. *Carbohydr. Res.* **340**, 417–428 (2005).
34. Emmanuel, V., Odile, B. & Céline, R. FTIR spectroscopy of woods: A new approach to study the weathering of the carving face of a sculpture. *Spectrochim Acta Mol. Biomol. Spectrosc.* **136**, 1255–1259 (2015).
35. Popescu, C. M. et al. Vibrational spectroscopy and X-ray diffraction methods to Establish the differences between hardwood and softwood. *Carbohydr. Polym.* **77**, 851–857 (2009).
36. Schwanninger, M. J. C. R. et al. Effects of short-time vibratory ball milling in the shape of FT-IR spectra of wood and cellulose. *Vib. Spectrosc.* **36**, 23–40 (2004).
37. Pandey, K. K. A study of chemical structure of soft and hardwood and wood polymers by FTIR spectroscopy. *J. Appl. Polym. Sci.* **71**, 1969–1975 (1999).
38. Mushtaq, Q. et al. Optimization of alkali treatment for production of fermentable sugars and phenolic compounds from potato Peel waste using topographical characterization and FTIR spectroscopy. *Molecules* **28**, 1–19 (2023).
39. Hong, T. et al. Applications of infrared spectroscopy in polysaccharide structural analysis: progress, challenge and perspective. *Food Chem. X*. **30**, 1–16 (2021).
40. Jing, X., Yang, C. & Zhang, L. Characterization and analysis of protein structures in oat Bran. *J. Food Sci.* **81**, 2337–2343 (2016).
41. Tamaki, Y. & Mazza, G. Rapid determination of lignin content of straw using fourier transform Mid-Infrared spectroscopy. *J. Agric. Food Chem.* **59**, 504–512 (2011).
42. Liu, R., Yu, H. & Huang, Y. Structure and morphology of cellulose in wheat straw. *Cellulose* **12**, 25–34 (2005).
43. Ghaffar, S. H. & Fan, M. Structural analysis for lignin characteristics in biomass straw. *Biomass Bioenerg.* **57**, 264–279 (2013).
44. Nurazzi, N. M. et al. Thermogravimetric analysis properties of cellulosic natural Fiber polymer composites: A review on influence of chemical treatments. *Polymers* **13**, 1–15 (2021).
45. Quan, C., Gao, N. & Song, Q. Pyrolysis of biomass components in a TGA and a fixed-bed reactor: thermochemical behaviors, kinetics, and product characterization. *J. Anal. Appl. Pyrol.* **121**, 84–92 (2016).
46. Liu, Q. et al. Interactions of biomass components during pyrolysis: a TG-FTIR study. *J. Anal. Appl. Pyrol.* **90**, 1–6 (2011).
47. Etale, A. et al. Cellulose: A Review of Water Interactions, Applications in Composites, and Water Treatment. *Chem Rev.*, 123, 1–33 (2023). (2023).
48. Mishra, R. K. & Vinu, R. Pyrolysis characteristics and kinetic investigation of waste groundnut shells using thermogravimetric analyzer, Py-FTIR, and Py-GC-MS. *J. Anal. Appl. Pyrol.* **179**, 1–14 (2024).
49. Wang, B. et al. Thermogravimetric and kinetic analysis of High-Temperature thermal conversion of pine wood sawdust under CO_2/Ar. *Energies* **14**, 1–15 (2021).
50. Poletto, M. Polypropylene-based wood-plastic composites: effect of using a coupling agent derived from a renewable resource. *Maderas Ciencia Y Tecnología*. **19**, 265–272 (2017). s.
51. Mallick, D. et al. Mechanistic investigation of pyrolysis kinetics of water hyacinth for biofuel employing isoconversional method. *Sustain. Energy Technol. Assessments*. **57**, 1–13 (2023).
52. Adeniyi, A., George, Iwuozor, K. O., Emenike, E., Chizitere, Adeyanju, C. A. & Ogunniyi, S. Mechanical and microstructural properties of Bio-composite produced from recycled polystyrene/chicken feather Biochar. *J. Renew. Energy Environ.* **11**, 1–8 (2024).
53. Nam, N. H., Ngoc, C. T. A. & Van Bay, T. Investigation on gasification of coffee husk in CO_2, H_2O, and mixed atmospheres. VJCH, 59, 775–780 (2021). (2021).
54. Linh, V. N., Van Dong, N. & Nam, N. H. Investigation on gasification of agricultural wastes: the case of macadamia husk. *VJCH* **59**, 599–605. https://doi.org/10.1002/vjch.202100011 (2021).
55. Bamisaye, A. et al. Maxakato N.W. H2SO4-treated and Raw watermelon waste bio-briquettes: comparative, eco-friendly and machine learning studies. *Fuel* **358**, 1–12 (2023).
56. PN-EN ISO 18134. Solid biofuels—Determination of moisture content—Drying method—Part 2:(2017).
57. PN-EN ISO 18123. Solid biofuels—Determination of volatile matter, (2016).
58. PN-EN ISO 18122. Solid biofuels—Determination of Ash Content, (2016).
59. PN-EN 15104. Solid Biofuels—Determination of Total Content of Carbon, Hydrogen and Nitrogen—Instrumental Methods. (2011).
60. PN-EN ISO 16948. Solid Biofuels—Determination of Total Content of Carbon, Hydrogen and Nitrogen. (2015).
61. PN-EN ISO 16994. Solid Biofuels—Determination of Total Content of Sulfur and Chlorine. (2016).
62. PN-EN ISO 1928. Solid mineral Fuels—Determination of gross calorific value by the bomb calorimetric method, and calculation of net calorific value., (2002).
63. Ekici, E. et al. Continuous flow pyrolysis of Virgin and waste polyolefins: a comparative study, process optimization and product characterization. *Front. Chem. Sci. Eng.* **18**, 1–17 (2024).
64. Howari, H. et al. Multi-Objective optimization for ranking waste biomass materials based on performance and emission parameters in a pyrolysis Process—An AHP–TOPSIS approach. *Sustainability* **15**, 1–19 (2023).
65. Durairaj, S., Sathiyasekar, K. & Ilangkumaran, M. Selection of alternate fuel for electrical power generator using hybrid multi criteria decision making technique. University Politehnica of Bucharest Scientific Bulletin Series C-Electrical Engineering and Computer Science, **78**, 247–258 (2016).
66. Hwang, C. L. & Yoon, K. *Multiple Attribute Decision Making: Methods and Applications* (Springer-, 1981).
67. Ahmad, S. et al. A hybrid approach using AHP–TOPSIS methods for ranking of soft computing techniques based on their attributes for prediction of solar radiation. *Environ. Chall.* **9**, 1–15 (2022).

Acknowledgements

The authors thank Dr. Magdalena Joka Yildiz for providing the Thermogravimetry Analysis instrument and its methodology.

Author contributions

I.A. conceptualization, I.A., G.Ł., G.Ś., G.Z. methodology, I.A., G.Ł., G.Ś., G.Z. data curation and interpretation, I.A., G.Ł., G.Ś., G.Z. investigation, I.A., G.Ł., G.Ś., G.Z. contributed to writing-original draft preparation and editing, G. Ł. supervision, G. Ł., I.A. funding.

Funding
This work was done as WZ-WB-IIŚ/4/2023 and WI/WB-IIŚ/8/2025. This research did not receive any specific grant from funding agencies in the public, commercial, or not-for-profit sectors.

Declarations

Competing interests
The authors declare no competing interests.

Additional information
Correspondence and requests for materials should be addressed to A.R.I.

Reprints and permissions information is available at www.nature.com/reprints.

Publisher's note Springer Nature remains neutral with regard to jurisdictional claims in published maps and institutional affiliations.